ISSN 8755-6839

SCIENCE OF **TSUNAMI HAZARDS**

Journal of Tsunami Society International

Volume 38 **Number 2** **2019**

WWW.TSUNAMISOCIETY.ORG

TSUNAMI SOCIETY INTERNATIONAL, 1741 Ala Moana Blvd. #70, Honolulu, HI 96815, USA.
SCIENCE OF TSUNAMI HAZARDS is a CERTIFIED OPEN ACCESS Journal included in the prestigious international academic journal database DOAJ, maintained by the University of Lund in Sweden with the support of the European Union. SCIENCE OF TSUNAMI HAZARDS is also preserved, archived and disseminated by the National Library, The Hague, NETHERLANDS, the Library of Congress, Washington D.C., USA, the Electronic Library of Los Alamos, National Laboratory, New Mexico, USA, the EBSCO Publishing databases and ELSEVIER Publishing in Amsterdam. The vast dissemination gives the journal additional global exposure and readership in 90% of the academic institutions worldwide, including nation-wide access to databases in more than 70 countries.

OBJECTIVE: Tsunami Society International publishes this interdisciplinary journal to increase and disseminate knowledge about tsunamis and their hazards.

DISCLAIMER: Although the articles in SCIENCE OF TSUNAMI HAZARDS have been technically reviewed by peers, Tsunami Society International is not responsible for the veracity of any statement, opinion or consequences.

Submit manuscripts of research papers, notes or letters to the Editor. If a research paper is accepted for publication the author(s) must submit a scan-ready manuscript, a Doc, TeX or a PDF file in the journal format. Issues of the journal are published electronically in PDF format. There is a minimal publication fee for authors who are members of Tsunami Society International for three years and slightly higher for non-members. Tsunami Society International members are notified by e-mail when a new issue is available. Permission to use figures, tables and brief excerpts from this journal in scientific and educational works is granted provided that the source is acknowledged.

Recent and all past journal issues are available at: http://www.TsunamiSociety.org CD-ROMs of past volumes may be purchased by contacting Tsunami Society International at postmaster@tsunamisociety.org Issues of the journal from 1982 thru 2005 are also available in PDF format at the U.S. Los Alamos National Laboratory Library http://epubs.lanl.gov/tsunami/

ISSN 8755-6839

SCIENCE OF TSUNAMI HAZARDS

Journal of Tsunami Society International

Volume 38 Number 2 2019

THE BEHAVIOR OF A TSUNAMI-LIKE WAVE PRODUCED BY DAM BREAK AND ITS RUN-UP ON 1:20 SLOPE

Benazir[1], Radianta Triatmadja[2*], Adam Pamudji Rahardjo[2], and Nur Yuwono[2]

[1]Doctoral Student at Dept of Civil and Environmental Engineering, Faculty of Engineering Universitas Gadjah Mada, Indonesia.
[2]Department of Civil and Environmental Engineering, Faculty of Engineering Universitas Gadjah Mada, Indonesia.
*Corresponding author: radianta@ugm.ac.id, Kompleks Yadara V/12 Babarsari Yogyakarta, Indonesia, 55281.

ABSTRACT

A solitary wave is commonly used in tsunami study for both physical and numerical models. A tsunami is categorized as a long wave which drastically changes its shape and speed when propagates in shallow water and land. In this paper, a physical model test of tsunami propagation based on Dam Break system to produce a tsunami-like wave was carried out. In a flume, finite reservoir length is set to sufficiently provide downstream length for propagation and run-up area. The downstream part is divided into two sections of bed configuration where it has flatbed as shallow water region and 1:20 of sloping beach model. The effect of the ratio of the reservoir depth to the initial downstream depth (d_0/d_1) is discussed. In addition, the tsunami inundation depth and run-up in land were also investigated. For comparison of results, numerical model similar to the physical one was conducted. The numerical model was based on a set of nonlinear shallow water equation that employed second-order explicit leap-frog finite difference scheme. The use of numerical approach using shallow water equation may not yield realistic results since the wave evolution in shallow water and coastal area has not sufficiently accommodated. The comparison between the models suggested that the numerical model consistently produce slightly higher run-up than its counterpart. This was probably due to the application of shallow water equation (SWE) in the numerical model which could not entirely solve vertical convection problems, breaking waves, and turbulence-related aspects that reduced run-ups energy. A fine

tuning method to improve the numerical model run-ups is necessary by introducing proper artificial energy reduction mechanism in the numerical model especially at breaking condition.

Keywords**:** *bore; modeling; long wave; dam break; inundation.*

1. INTRODUCTION

Tsunami that is triggered by tectonic activity, especially earthquake on the ocean floor is relatively small in amplitude at fault location or in deep sea. Its velocity decreases dramatically when the wave reaches the shallow water with decreasing water depth. In this phase, the wave height is increased and suddenly transformed to breaking wave. Since tsunami is a long wave it makes the flow effortlessly towards the mainland and cause damage and flooding. Tsunami surge that propagates in shallow water and coastal plain is in some criteria like the wave that was produced by the failure of a reservoir or dam break (Chanson, 2006). Based on some documentation in tsunami event, the wave characteristics tend to break as bore when traveling to the coastline (nearshore) i.e. the wave propagation in Kuji Bay during Tsunami Tohoku 2011. Previously, Shuto (1997) observed Tsunami at Showa 1933 which indicated that for tsunami with a wave height of more than 4 m, a plunging breaking type occurs in shallow water.

The first study of single long wave study approaching a coastal slope was, among others, performed by Hall & Watt (1953). This physical experiment realized the 1+1 one-dimensional long wave theory, which generated long wave over a constant depth, evolving to a constant depth, and then climbing a sloping beach. Miller (1968) also conducted laboratory work by tested wave propagation on four slope variations. The development of tsunami hydrodynamics began in the early 1980s that focused solitary waves as the initial condition (Synolakis & Bernard, 2006). In the late 1980s, Synolakis (1986) and Synolakis (1987) accomplished the Initial Value Problem (IVP) of the Nonlinear Shallow Water Equation (NLSWE) for solitary wave propagation over a constant water depth until run-up to the sloping beach. Synolakis (1987) derived the equation which is then known as "Run-up Law" for solitary wave propagation on the sloping beach and compared it with relevant laboratory results. The discussion about tsunami waveform during its propagation over constant depth was also done by Yeh and Ghazali (1986). It seemed that breaking and non-breaking condition depended on the initial condition of a simulation setup. This research aims to discuss tsunami-like waveforms over constant depth and sloping beach that was initiated by Dam Break method.

1. LITERATURE REVIEW

Tsunami run-up formulae have been developed using various approaches. Early in its development, the run-up relationships were associated with wavelength and wave height at the shore as done by Kaplan (1955); Shuto (1967); and Togashi (1981). Freeman and Le Mehaute (1964) predicted run-up that was affected by the horizontal velocity component when it reached the shoreline without considering beach slope variable. The derivation of an analytical equation from the laboratory work by using shallow water wave theory was also done by Synolakis (1986) and (1987). Li & Raichlen (2003) and Zhao et al. (2012) also conducted a study of the tsunami

run-up model in which the energy variables changed when the wave reached the coastal land. The common run-up formulae used today are shown in Table 1.

Long wave amplitude increases as it travels in sloping shallow water until the wave eventually breaks. Bore height is usually the main parameter associated with the run-up process. Baldock & Holmes (1999) analytically derived the formula (Table 1) based on run-up and run-down (swash) oscillation with a bore waveform. In obtaining the equation, they also studied the energy transfer around the coastline. The equation describes that the unsaturated run-up (i.e. the same run-up as the first swash) as a function of flow velocity or bore height (H_B). The coefficient of C_k is kinetic energy converted into potential energy during run-up which equals 2. Then, it indicates that the run-up height is twice the bore height ($R = 2H_B$). This coefficient is the same as in Yeh et al. (1989) which is called bore collapse.

Table 1. The existing non-dimensional tsunami run-up equations.

Waveform	Non-Dimensional Run-up (R/d_1)	Equation No.	Reference
Solitary	$11(\beta)^{0.67}(H/d_1)^{1.9(\beta)^{0.35}}, \beta = 5° - 12°$ $3.05(\beta)^{-0.13}(H/d_1)^{1.15(\beta)^{0.02}}, \beta = 12° - 45°$	(1)	Hall & Watt (1953)
Solitary	$2.831\sqrt{cot\beta}\left(\frac{H}{d_1}\right)^{1.25}$	(2)	Synolakis (1987)
Solitary	$1.109\left(H/d\right)^{0.582} \quad (max)$ $0.918\left(H/d\right)^{0.606} \quad (avg)$	(3a) (3b)	Synolakis (1987)
N-wave	$3.3\varepsilon_g p_0^{\frac{1}{4}} Q(L,\gamma_s)\frac{R_{sol}}{d_1}$	(4)	Tadepalli & Synolakis (1996)
Bore	$\frac{U_0{}^2}{2gd_1} = \frac{C_k{}^2 H_B}{2d_1}$	(5)	Baldock & Holmes (1999)
Bore	$\frac{U^{*2}}{2gd_1}$	(6)	Shen & Meyer (1963)
N-Wave	$3.86\sqrt{cot\beta}\left(\frac{H}{d_1}\right)^{1.25}$	(7)	Tadepalli & Synolakis (1994)
Double N-Wave	$4.55\sqrt{cot\beta}\left(\frac{H}{d_1}\right)^{1.25}$	(8)	Tadepalli & Synolakis (1994)

2. RESEARCH METHOD

A physical simulation of tsunami propagation and run-up using Dam Break method was implemented in a laboratory flume. This simulation focused on wave propagation in constant depth or shallow water region, wave propagation on shore, run-up and inundation. The mechanism of tsunami generation and propagation using Dam Break method and its variables are shown in Figure 1. This physical work was performed in a channel of 15.00 m long by 0.60 m wide and 0.44 m in height. The downstream depth () represented the constant depth of the sea water near the coast. As can be seen in the figure that the channel was divided into two regions, i.e. the upstream region of 4 m as a reservoir and downstream region of 11 m as a coastal model profile which was separated by a sluice gate. Along the downstream region, there was 3 m long horizontal bottom profile (constant depth zone) as shallow water area followed by a beach model (sloping zone) with a uniform slope of 1:20 which may be categorized as a mild slope. Thus, the source of tsunami generation (gate) was 4 m for = 0.05 m and 5 m for = 0.10 m from the coastline. The experiment was set up to obtain typical bore formations and to get more complete data to examine the bore characteristics resulting from a Dam Break method, especially, when the bore propagated on a constant depth before run-up on land. This method has been commonly used to model tsunami that arrived in shallow water region and on land such as by Chanson (2005); Triatmadja & Nurhasanah (2012); and Triatmadja & Benazir (2014).

Using Dam Break method, waves were formed by the rapid released of the gate (using quickly released mechanism). The gate opening depended on the load that was connected to the gate. The load weight can be calculated based on Triatmadja (2010) for high opening speeds so that the gate can be considered instantaneously (ranging from 0.1-0.4 seconds depending on the reservoir depth). The wave behavior, including the height and velocity, downstream of the channel was affected by the reservoir depth as well as the downstream depth. The difference between the reservoir and the downstream depth defined the generated wave height while the ratio of reservoir depth to the downstream depth affect more specifically on the bore behavior. Based on Yeh et al. (1989), the behavior of bore formation was presented at the initial simulation for parameter , which was classified as fully developed bore and undular bore. In this study, two variations for were applied, i.e. 0.05 m and 0.10 m which were tested with four reservoir depths, i.e. 0.30 m, 0.25 m, 0.20 m, and 0.15 m. A mini pump was used to make sure that the depth in both regions has sufficiently accurate as shown in Figure 2 (right).

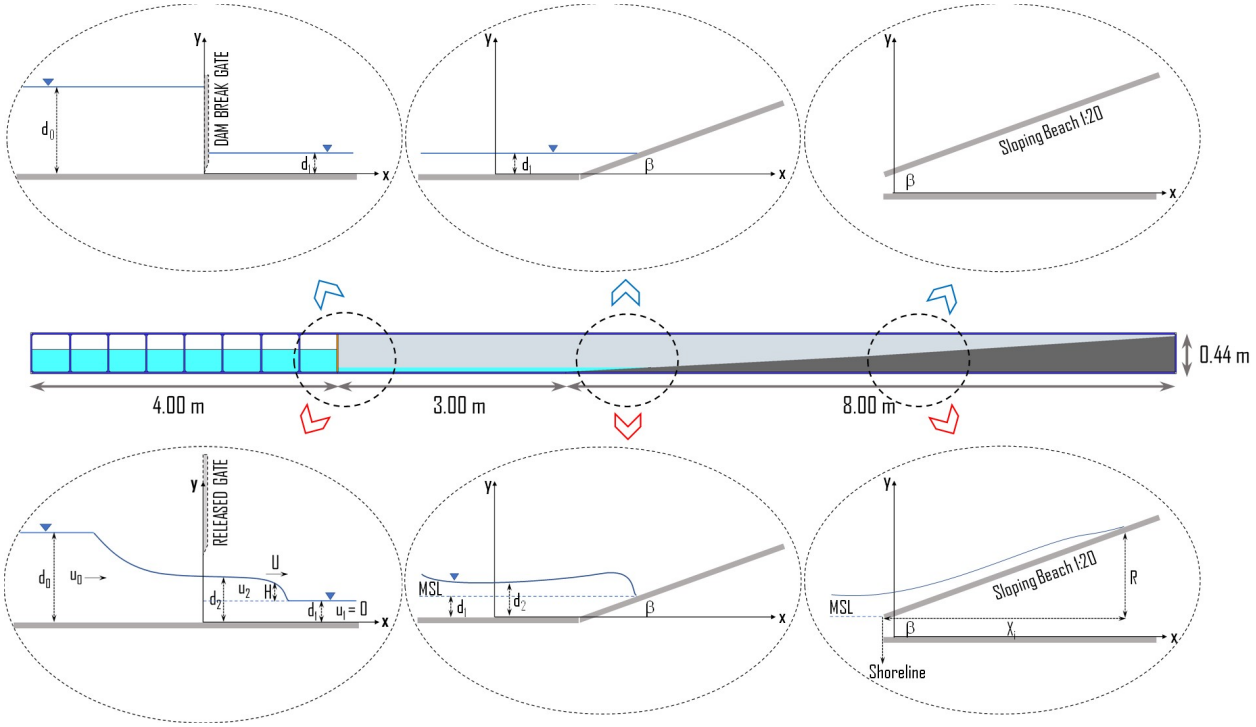

Figure 1. The mechanism of wave generation using Dam Break method and its variables

Wave probes were used to retrieve the water fluctuation over time. There were four sensors used in this test, which were placed at 2, 3, 4, and 5 m from the dam gate as portrayed in Figure 2 (left). The sensors were calibrated before they were used for data acquisition.

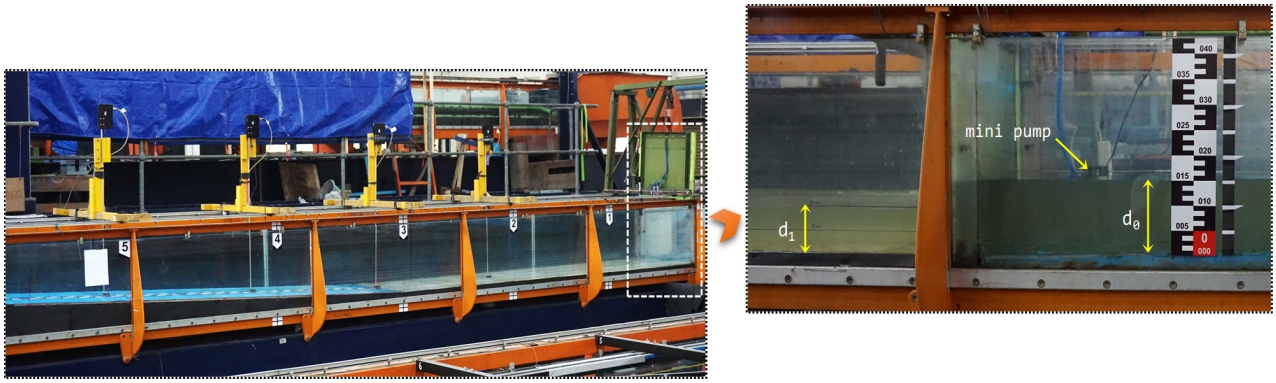

Figure 2. The downstream and upstream of wave flume

To study the wave behavior that traveled along the channel, five cameras (Cam) were placed in the simulation area. Cam-1 was placed near the dam gate to record the waveform when the gate was opened. Cam-2 was positioned in the upstream of the channel to record the wave propagation, especially when it began to climb the coastal slope. Cam-3 was used to observe details of wave propagation over the constant depth and when it began climbing on the coastal slope. This camera

was capable of recording video up to 60 fps (frame per second) with Full High Definition (FHD) quality. For recording the entire simulation area, Cam-4 was placed farther away from Cam-3. Finally, for close examination of the inundation height and length, the simulation was equipped with Cam-5.

Numerical simulation was performed and was verified using the physical model. The same cases were simulated using the main program of Goto et al. (1997) and Imamura et al. (2006). The program was slightly modified where some additional input-output facilities were added for convenience and rewrote the program in Visual Basic .Net programming language. The program uses second-order explicit leap-frog finite difference scheme to discretize a set of Nonlinear Shallow Water Equation (NSWE). For the propagation of tsunami in the shallow water, the horizontal eddy turbulence terms are negligible as compared with the bottom friction. The equations are written in Cartesian coordinate as (Imamura et al., 2006):

$$\frac{\partial \eta}{\partial t} + \frac{\partial M}{\partial x} + \frac{\partial N}{\partial y} = 0 \tag{9a}$$

$$\frac{\partial M}{\partial t} + \frac{\partial}{\partial x}\left(\frac{M^2}{D}\right) + \frac{\partial}{\partial y}\left(\frac{MN}{D}\right) + gD\frac{\partial \eta}{\partial x} + \frac{\tau_x}{\rho} = 0 \tag{9b}$$

$$\frac{\partial M}{\partial t} + \frac{\partial}{\partial x}\left(\frac{MN}{D}\right) + \frac{\partial}{\partial y}\left(\frac{N^2}{D}\right) + gD\frac{\partial \eta}{\partial y} + \frac{\tau_y}{\rho} = 0 \tag{9c}$$

$D = h + \eta$ is the total water depth where h is the still water depth and η is the sea surface elevation. M and N are the water velocity fluxes in the x and y directions, respectively

$$M = \int_h^\eta u dz = u(h + \eta) = uD \tag{10a}$$

$$N = \int_h^\eta v dz = v(h + \eta) = vD \tag{10b}$$

Bottom friction in the x and y direction are respectively represented by terms τ_x and τ_y, which is a function of friction coefficient *f*. This coefficient can be computed from Manning roughness (n_0) by the following relationship

$$n_0 = \sqrt{\frac{fD^{1/3}}{2g}} \rightarrow f = \frac{{n_0}^2 2g}{D^{1/3}} \tag{11}$$

Eq. (11) describes that the friction coefficient increases when the total water depth decreases. Manning roughness is usually chosen as a constant for a given condition of sea bottom, then the bottom friction terms are expressed by

$$\frac{\tau_x}{\rho} = \frac{1}{2}\frac{f}{D^2} M\sqrt{M^2 + N^2} \tag{12a}$$

$$\frac{\tau_y}{\rho} = \frac{1}{2}\frac{f}{D^2} N\sqrt{M^2 + N^2} \tag{12b}$$

In this research, Manning coefficient () of 0.012 was used to describe the bed slope that was made of plywood. Other numerical parameters are listed in Table 2.

Table 2. Parameters that were used in the numerical model

Grid Numbers		Grid Size (m)		DT	Total Time
x	y	x	y	(s)	(s)
1500	60	0.01	0.01	0.0025	180

3. RESULT AND DISCUSSION

1.Tsunami Generation on Laboratory Scale using Dam Break Method

The tsunami flowed easily towards mainland due to its long wave characteristics and normally caused flooding. Based on some criteria, tsunami surge that propagates in shallow water and coastal plain is similar to the wave that was produced by the failure of reservoir or dam break (Chanson, 2006). Figure 3 shows a wave propagation stage from a laboratory test where = 2.0 and = 0.10 m. The front velocity was relatively high when it traveled at the constant depth depending on . Figure 3 (top left) shows the wave front location at = 2 m at = 1.07 s after which the wave propagated at the sloping zone and reached the coastline, i.e. at = 5 m at = 3.07 s. The waves propagated faster for the same when > 2.0. On land, the front velocity decreased and continued to climb the beach slope profile to the maximum run-up at = 7.63 m followed by the run-down phase.

he wave height fluctuated during the travel time for each model of beach profile. As mentioned earlier the wave height was defined by the difference between the and . The larger was the value of and yielded the higher wave heights in the downstream. In addition, the recorded wave fluctuations also vary over the measurement locations. In shallow water, the recorded wave was relatively smaller than on land. The change in wave height was caused by changes in water depth or shoaling process. It followed by a condition where the wave crest became unstable which subsequently turns into breaking waves. It should be noted that when the wave height reached the maximum conditions on the ground, the front velocity decreased drastically as also observed by Lukkunaprasit et al. (2009). The vertical release of the gate on Dam Break method caused the flow below the gate to advance first which cause water to jump downstream of it. For a region close to the gate and in a very short time, such impulse affects the wave generation. For more details, the water fluctuations along the channel with two downstream depth variations are shown in Figure 4. Based on the measurement along the channel, it was found that the waves were higher on land rather than in the water.

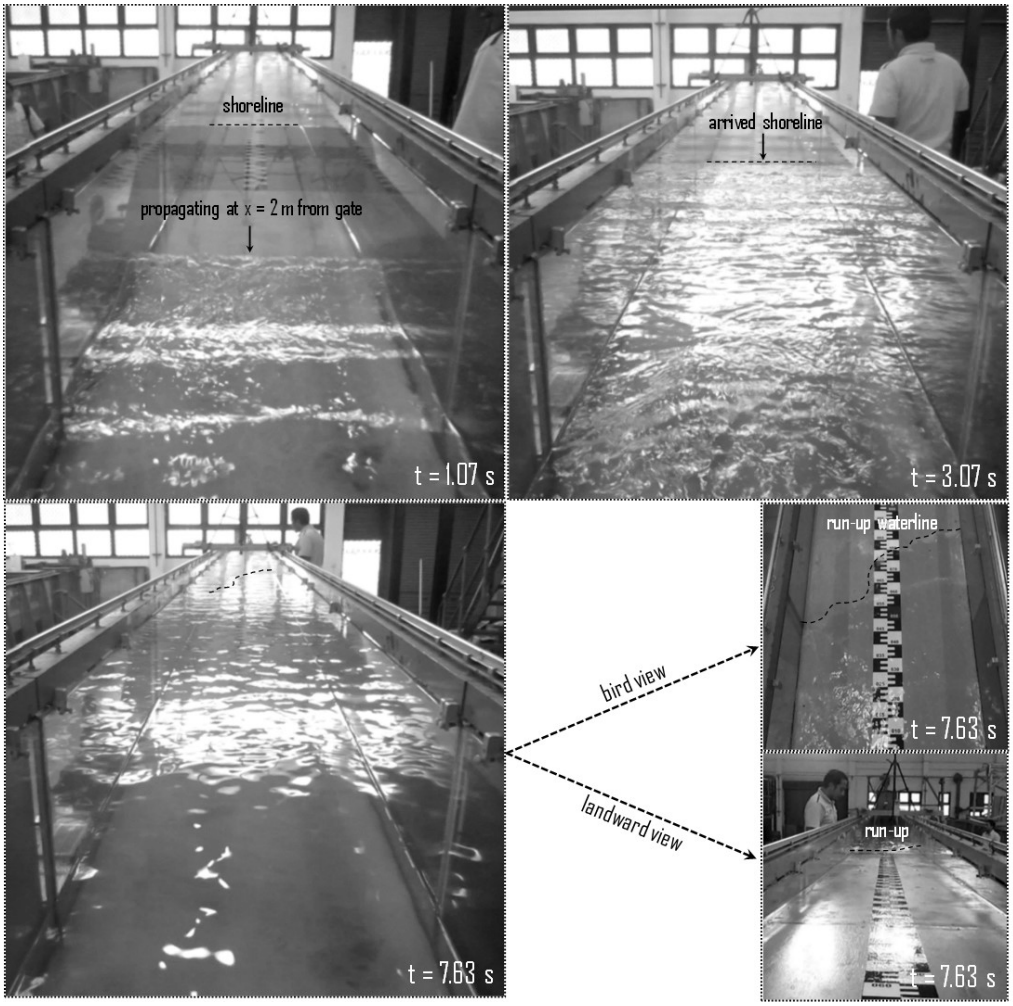

Figure 3. Surge resulted from Dam Break method in wave flume for = 2.0 and = 0.10 m

he wave height fluctuated during the travel time for each model of beach profile. As mentioned earlier the wave height was defined by the difference between the and . The larger was the value of and yielded the higher wave heights in the downstream. In addition, the recorded wave fluctuations also vary over the measurement locations. In shallow water, the recorded wave was relatively smaller than on land. The change in wave height was caused by changes in water depth or shoaling process. It followed by a condition where the wave crest became unstable which subsequently turns into breaking waves. It should be noted that when the wave height reached the maximum conditions on the ground, the front velocity decreased drastically as also observed by Lukkunaprasit et al. (2009). The vertical release of the gate on Dam Break method caused the flow below the gate to advance first which cause water to jump downstream of it. For a region close to the gate and in a very short time, such impulse affects the wave generation. For more details, the water fluctuations along the channel with two downstream depth variations are shown in Figure 4. Based on the measurement along the channel, it was found that the waves were higher on land rather than in the water.

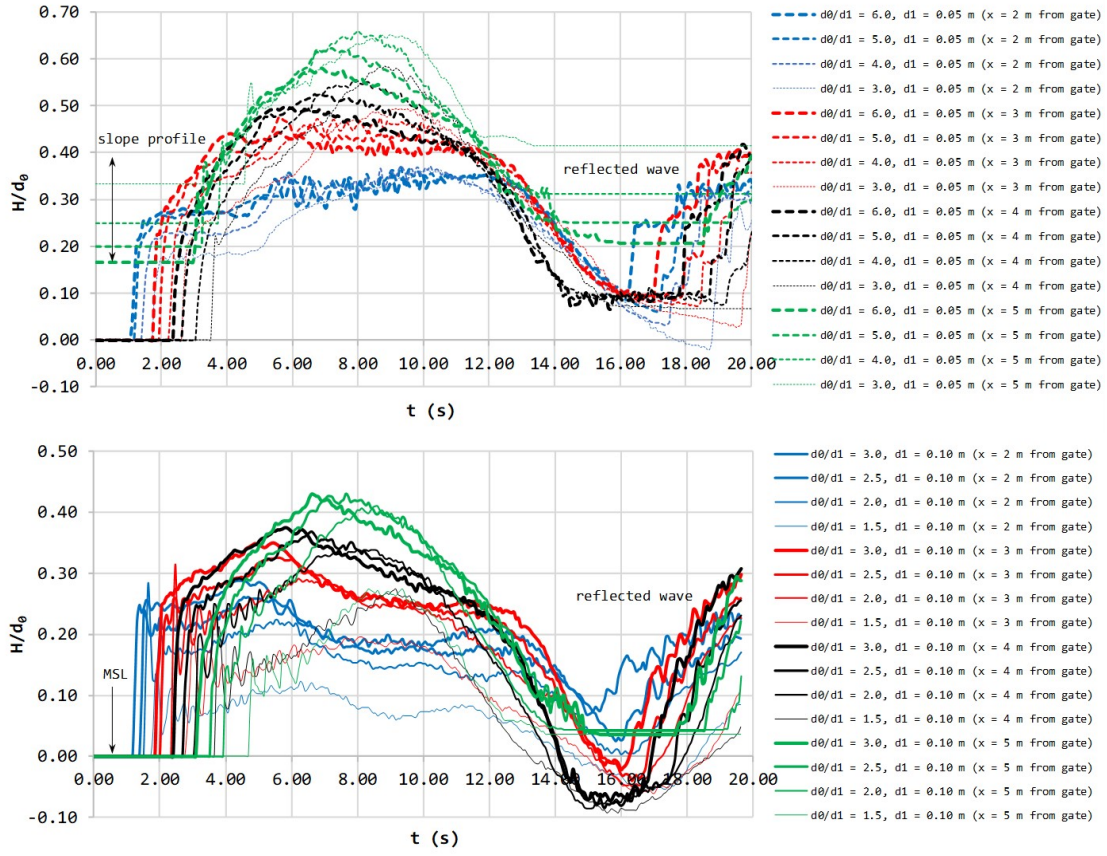

T

Figure 4. Water fluctuation along the channel by physical model tests for = 0.05 m (above) and 0.10 m (below).

The simulation of tsunami model by Dam Break approach requires an adequately long channel to accommodate run-up and run-down processes. However, if the study concern only to the surge front force parameters during run-up as done by Triatmadja & Nurhasanah (2012) and Triatmadja & Benazir (2014), longer channel may not be necessary. In this study, run-up and run-down processes were observed, where the reflected waves from the upstream end of the channel should not be allowed to affect the result. To satisfy this condition, the reservoir depth used was = 0.30 m, 0.25 m, 0.20 m, and 0.15 m whilst the reservoir length was adjusted to minimize the effect of upstream wall reflection on run-up and run-down. In the previous research schemes (Benazir et al. 2016a and 2016b), the reservoir length was 7.90 m which was reduced to 4.00 m in the present research. With these adjustments, the reflection occurred at the time when the run-down process ends. This allowed for an additional mechanism to totally remove the reflection (due to the upstream wall of the channel) by adding one more gate at downstream of the main gate as done by Kuswandi et al. (2017).

1.Wave Propagation in Constant Depth and Sloping Zone

Observations on the physical model of wave propagation in constant water were carried out. Four types of initial waveform were simulated at two different downstream depths (= 0.05 m and = 0.10 m) so that there were 8 (eight) waveforms with different height and behavior. The observation was repeated three times for each scenario and the results are shown in Figure 5. The parameter was used to discuss the waveforms.

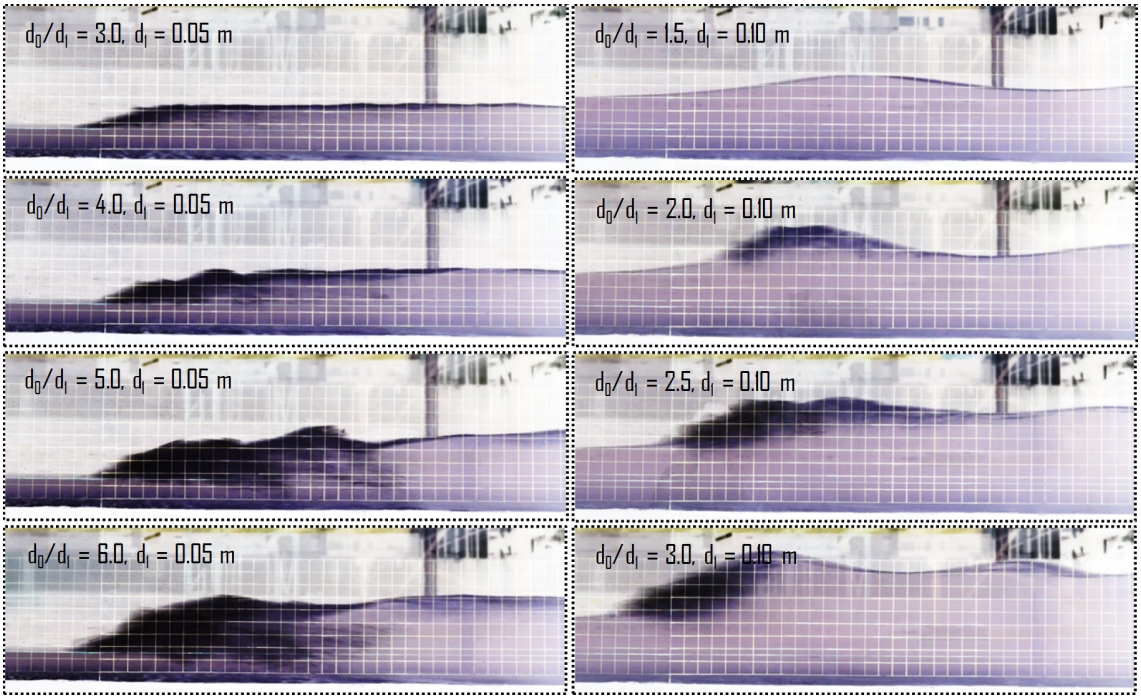

Figure 5. Bore variations in constant depth at = 2 m for all scenarios of the tested model (grid size is 0.02 m)

Based on visual observation, at x = 2 m from the source, the waveforms were almost entirely bore, except for d_0/d_1 = 1.5 (Fig. 5). This indicates that the developed bore was formed with the $d_0/d_1 \geq 2.0$. When $d_0/d_1 < 2.0$ such as for d_0/d_1 = 1.5 as shown in Figure 5, undular bore type was produced. This is due to the linear effect of significant frequency dispersion (Yeh & Ghazali, 1986). The undular bore transformation occurred when it traveled in the reducing depth (Fig. 6).

Figure 5 shows the shape of the wave fronts that was fully broken with high turbulence for all d_0/d_1 = 6.0, d_0/d_1 = 5.0, d_0/d_1 = 4.0, and d_0/d_1 = 3.0. The difference was apparent from the scale of the bore strength, such as for d_0/d_1 = 6.0 and d_0/d_1 = 5.0. According to Yeh et al. (1989), the scale of bore strength in the natural coast is limited by the mechanism of wave breaking. With the downstream depth of d_1 = 0.10 m, the strength ranged from d_0/d_1 = 1.5 to d_0/d_1 = 3.0 where the bore formation was partially developed (except for d_0/d_1 = 1.5). This partly developed bore was strongly turbulent (breaking wave) at the front of the bore whilst in the rear side such formation was not noticeable. However, the partly developed bore

formation was later transformed into fully developed bore during its travel as the depth reduced, as shown in Figure 7 for d_0/d_1 = 2.0. For d_0/d_1 > 2.0, the transformation to fully developed bore was indicated by its form which was more transient with higher turbulence.

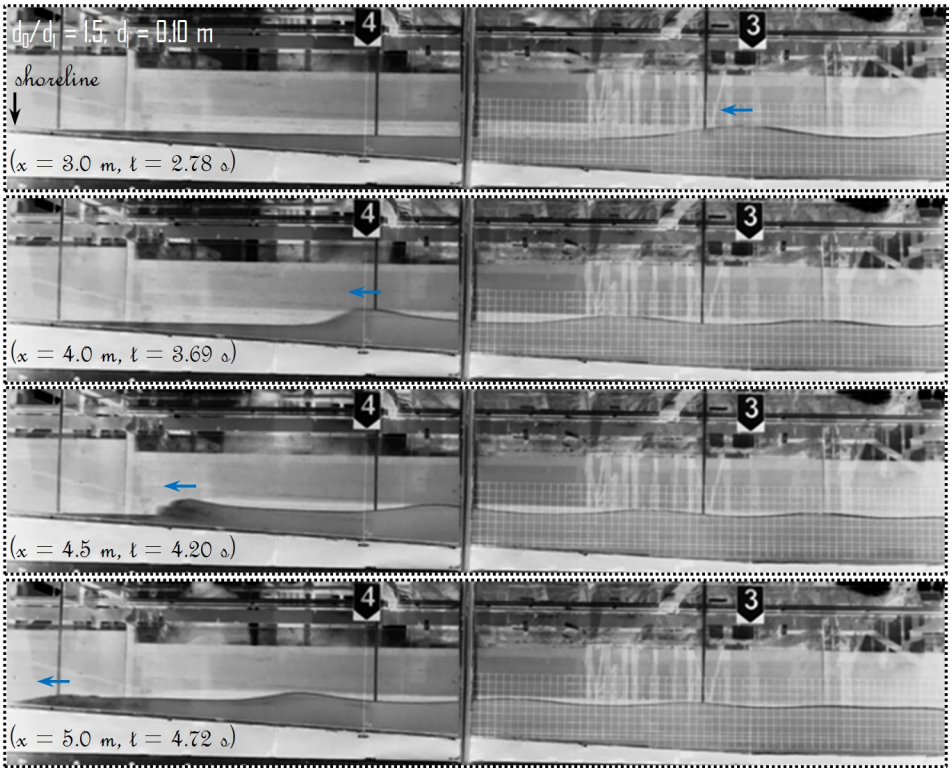

Figure 6. Wave propagation and transformation in sloping zone for d_0/d_1= 1.5 and d_1= 0.10 m

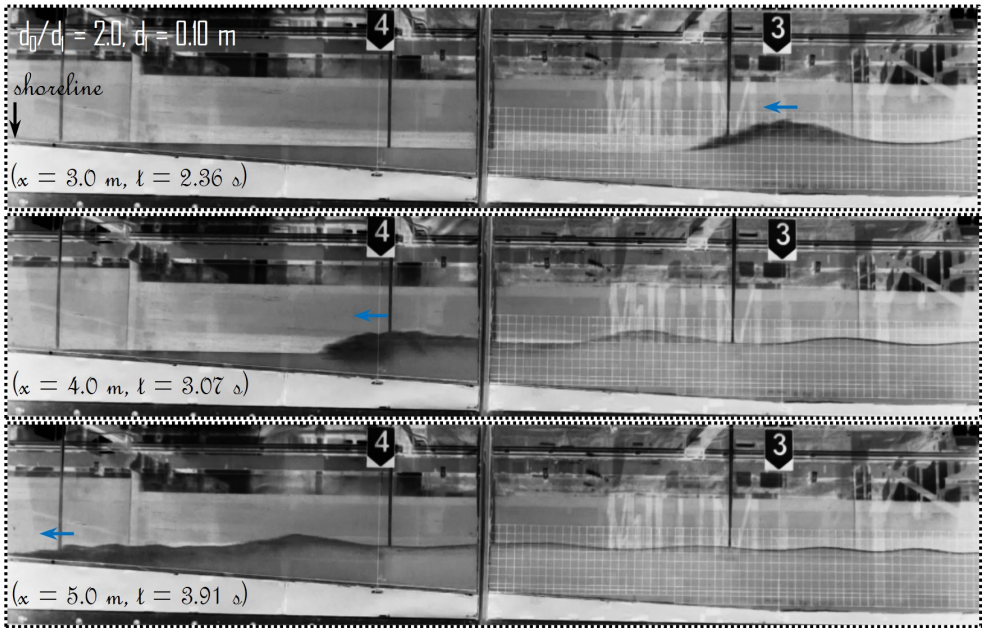

Figure 7. Formation of fully developed bore for d_0/d_1= 2.0 in the sloping zone

In Yeh & Ghazali (1986), Yeh et al. (1989), and Yeh (1991), the space for bore to develop after its generation (the length of constant bottom profile) was limited to 0.4 m. In this research, the length of this profile was 3 m or totally 4 m for = 0.05 m and 5 m for = 0.10 m including the additional sloping zone. Therefore, the undular form and partly developed bore may develop into fully developed bore when the wave travels to the beach. The total depths fluctuations at the constant depth zone depending on and are given in Figure 8.

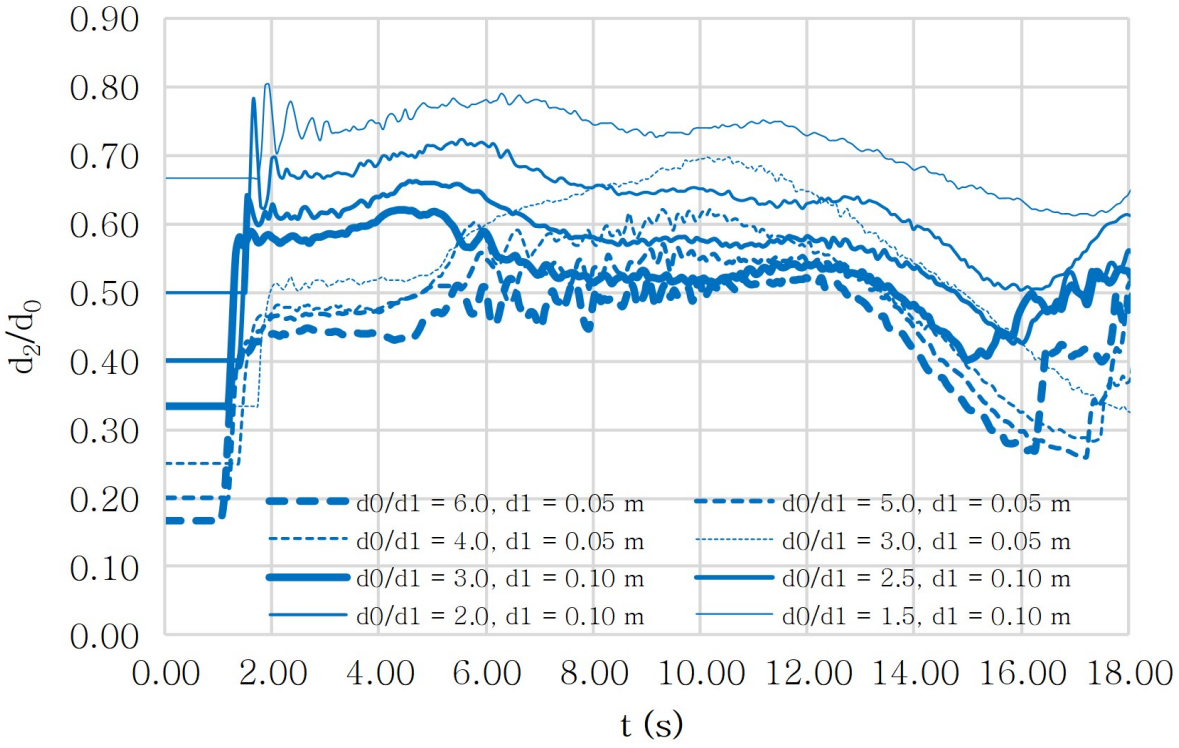

Figure 8. Fluctuations of total depth over time at constant depth zone for d_1 = 0.05 m (dash line) and d_1 = 0.10 m (solid line)

The front velocity in constant depth zone was given as a function of total depth of water (d_2) in Figure 9. The front velocity at d_1 = 0.10 m was greater than d_1 = 0.05 m and the measured velocity was plotted in Figure 9 against d_2. The analytical solutions from Chanson (2005) or (2006) predicted a very similar velocity for both d_1 = 0.10 m and d_1 = 0.05. The analytical line calculated based on Chanson's solutions has been extended to $d_0 = d_2 = d_1$ when theoretically the velocity of the surge front is $U = \sqrt{gd_2}$. This is the minimum theoretical velocity of the surge front in this experimental case. Other experimental data of Dam break surge velocities from Arnason et al. (2009) are also plotted in Figure 9. Arnason et al. (2009) experiment agreed with analytical solutions (calculated by the authors based on Arnason's data). They used d_1 = 0.02 m whilst d_0 varied from 0.10 to 0.30 m.

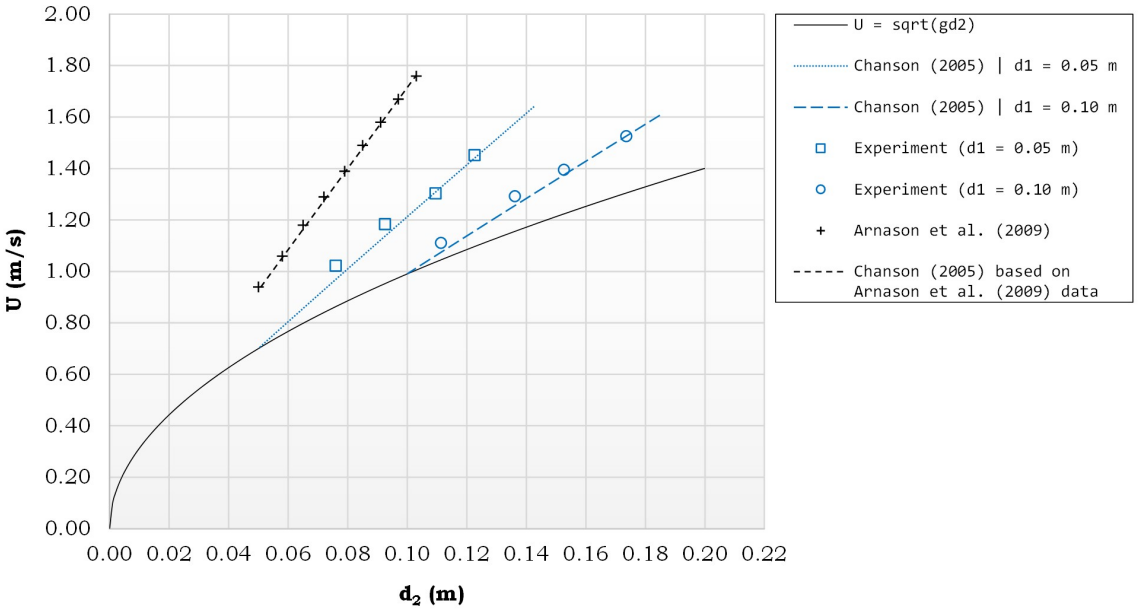

Figure 9. The relationship of front velocity and total depth of wave at a constant depth

1. Tsunami Run-up on Uniformly Sloping Beach 1:20

The surge velocity decreases as the influence of roughness and the effect of beach slope become more dominant. Figure 10 shows the surge velocity in the coastal area of the present model, which was calculated based on surge propagation in between = 4 m and x = 6 m for = 0.05 m and in between = 5 m and x = 7 m for = 0.10 m on dry land. It is seen that the wave Froude number for = 0.05 m was less than for = 0.10 m for the same . For the same the Froude number of the surge was greater at higher . The difference is more pronounced at lower . One of the reason is due to more turbulence and hence more energy dissipation at smaller or shallower water. In this case, was the inundation depth at the coastline.

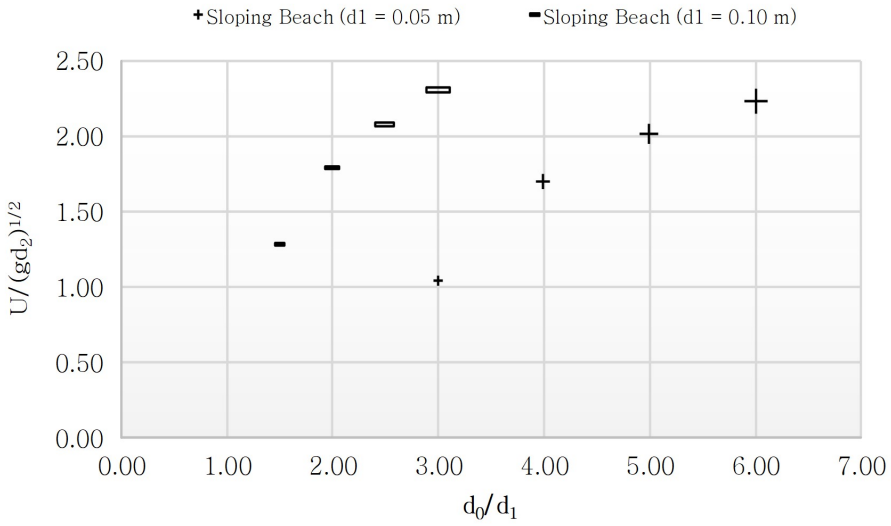

Figure 10. Front velocity in the coastal area

To compare between the physical, the numerical model results and with some analytical solutions, a non-dimensional relationship namely H/d_1 and R/d_1 parameters were used. The experimental data and analytical solutions of run-up are plotted in Figure 11. The variable H is the wave height $(d_2 - d_1)$ in shallow water, i.e. at x = 2 m in the present physical and numerical experiment and the solitary wave height in all other experiments. The run-up is represented by R.

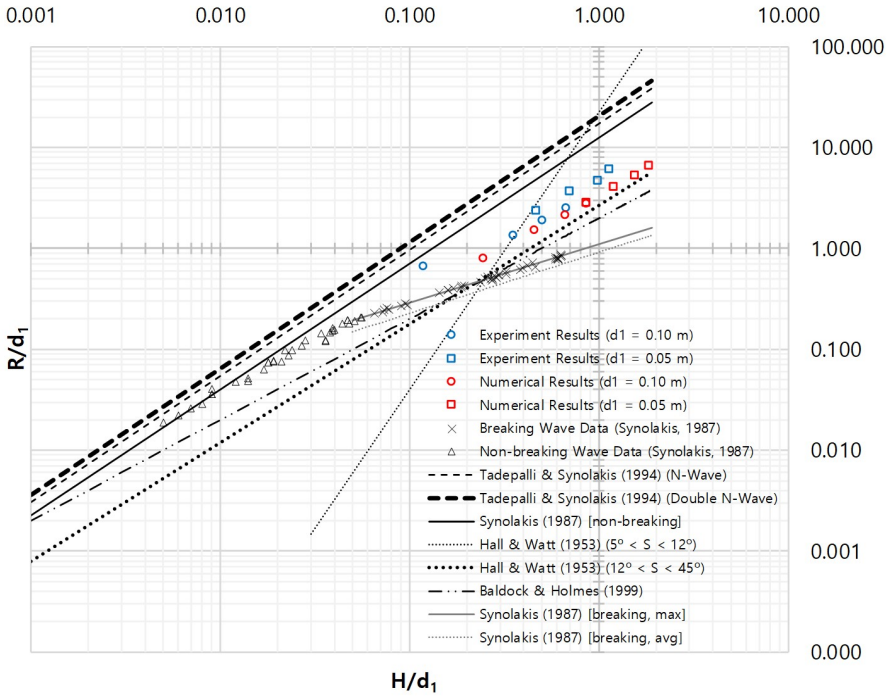

Figure 11. The relation of tsunami run-up on uniformly sloping beach and the wave height in water depth.

Figure 12 shows the maximum water level condition at different instants and at all recorded points along the slope of the beach. As can be seen in the figure that the numerical solutions are in general higher than the physical experiment for all d_0/d_1.

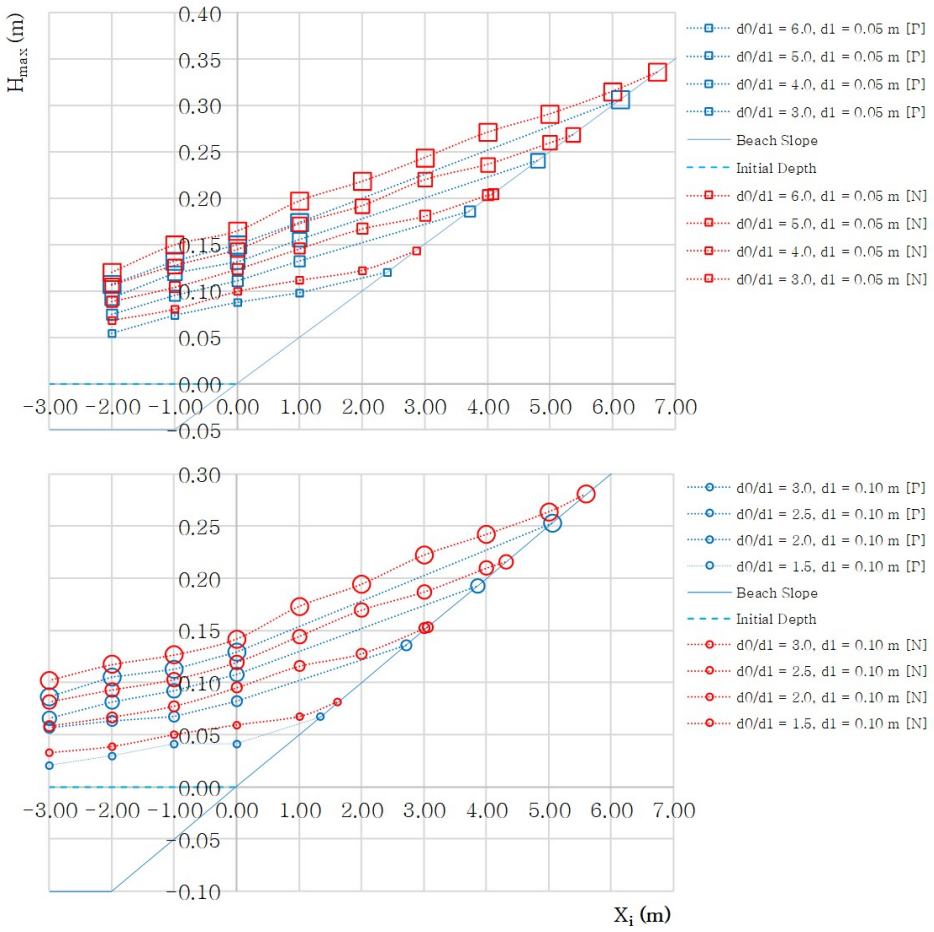

Figure 12. Comparison of physical and numerical models maximum water level along the beach slope.

The Shallow Water Equation (SWE) that assumes hydrostatic field pressure across the vertical is good enough to demonstrate tsunami motion. This is because tsunami has a larger horizontal length scale characteristic than the vertical length scale. In non-breaking waveforms conditions such as solitary and cnoidal waves, the SWE model can predict the run-up height and the run-up process in the coastal plain (Synolakis, 1991); (Liu, et al., 1991). However, when breaking wave occurs, the SWE cannot predict the run-up motion accurately as indicated in Figure 12. This suggests that the numerical solutions have not been able to accommodate the loss of energy (due to turbulence of breaking wave) during the propagation and run-ups. An additional artificial energy loss is required in the numerical scheme. As mentioned in the preceding section the typical wave resulted from Dam Break method is highly turbulence. Thus, the numerical model without artificial energy reduction based on SWE produced higher results or run-up than the physical model data. The run-ups difference was in between 9.64 and 20.61%.

A similar condition was also experienced in a study conducted by Hibberd & Peregrine (1979). They mentioned that such discrepancy was due to the effect of bottom friction which has not been properly addressed. Previously, Miller (1968) mentioned that besides coastal slope factors, bottom roughness also plays a role in determining run-up. This implied that in real cases, energy loss due to bottom roughness needs to be considered. Later, a modification to the Hibberd & Peregrine (1979) model was carried out by Packwood & Peregrine (1981) by adding the Chezy term to accommodate bottom roughness. However, the physical model by Miller (1968) was still lower than the numerical model which has not been fully explained by Packwood & Peregrine (1981).

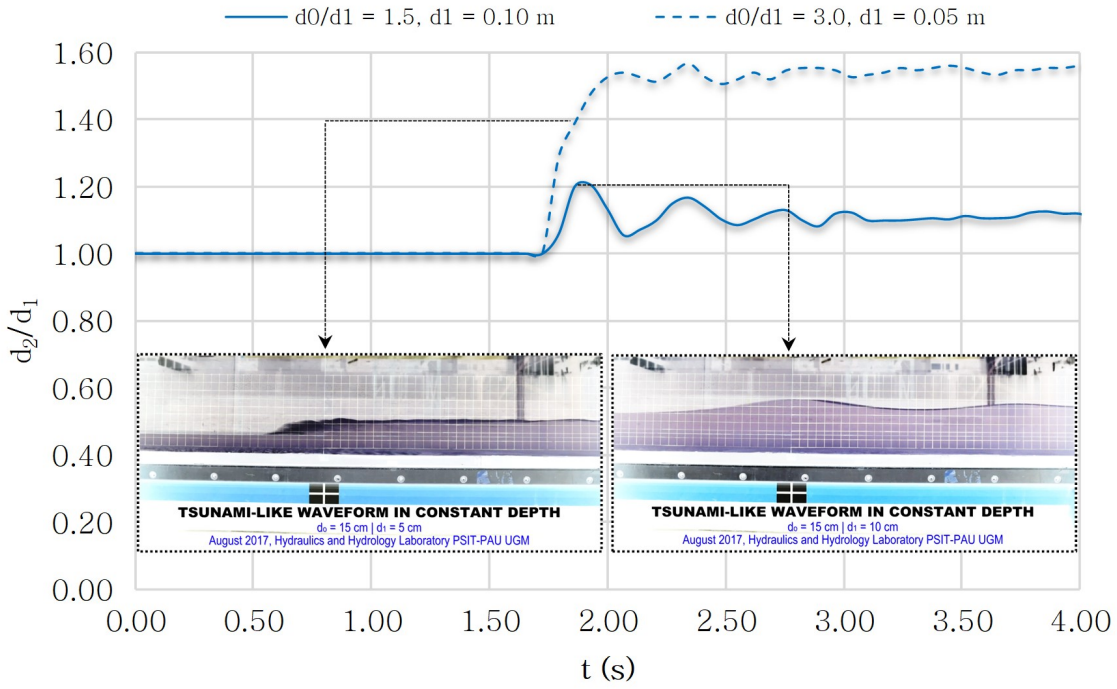

Figure 13. Typical of bore traveling in different water depth

In Figure 11, analytical and empirical solutions from some previous studies are depicted. The Run-up Law that was proposed by Synolakis (1987) is applicable for non-breaking solitary run-up. The theoretical run-up water level was above both the present physical and numerical models. This higher estimate was also experienced by Zelt (1991) when comparing the results of three models. The non-dispersive model produced higher run-up than both the dispersive model and physical experiment. In addition to Run-up Law, Synolakis (1987) also proposed the maximum and average run-up for breaking waves. These equations are also plotted in Figure 11. Synolakis (1987) solution for breaking wave was below both the present numerical and physical model results. Different type of waveforms or surge, namely solitary and bore, were most likely the reason for this deviation. This can be explained by focusing on the physical model data for H/d_1 = 0.118 which yields R/d_1 = 0.672 and it tends to approach the theoretical line of Run-up Law. The value of H/d_1 = 0.118 is produced when d_0/d_1 = 1.5 and d_1 = 0.10 m. This condition produced undular bore type which did not break. These two series or wave train are shown in Figure 13. The undular bore type, however, changed to breaking wave as it approached the shore (Figure 6) and released some of its energy.

Other solutions in Figure 11 also deviate from both the present numerical and physical results. Similarly, this was probably due to different characteristics of the incoming wave such as wind wave, solitary, N-wave and Double N-Wave by Baldock & Holmes (1999), Hall & Watt (1953), and Tadepalli & Synolakis (1994), respectively.

Other solutions in Figure 11 also deviate from both the present numerical and physical results. Similarly, this was probably due to different characteristics of the incoming wave such as wind wave, solitary, N-wave and Double N-Wave by Baldo

1. CONCLUSION AND RECOMMENDATION

The generation of tsunami using the Dam Break method produced surge wave that breaks in shallow water and inland, similar to tsunami that approaches and finally arrives on the coast (run-up mode). The behavior of tsunami surge that propagates in water and land by using Dam Break method depends on the reservoir depth and downstream depth. At a constant depth, when $d_0/d_1 \geq 2.0$ the surge wave produced fully developed bore and partly developed bore categories while the undular bore category was formed when $d_0/d_1 < 2.0$. The front celerity agree with the analytical solution of Chanson (2005). The comparison between physical and numerical models suggested that the numerical model consistently produce slightly higher run-up than its counterpart. This was probably due to the application of shallow water equation (SWE) in the numerical model that is unable to solve vertical convection problems, breaking waves, and turbulence-related aspects. Nevertheless, important characteristics in tsunami simulations such as propagation, run-up, and inundation have been successfully simulated by the addition of terms to the governing equations based on the SWE.

ACKNOWLEDGMENT

The research was fully funded by Lembaga Pengelolaan Dana Pendidikan (LPDP) Kementerian Keuangan Republik Indonesia via Scholarship of Indonesia Education (BPI). We would like to express our sincere gratitude for the funding.

REFERENCES

Arnason, H., Petroff, C. & Yeh, H., 2009. Tsunami Bore Impingement onto a Vertical Column. *Journal of Disaster Research,* 4(6), pp. 391-403.

Baldock, T. E. & Holmes, P., 1999. Simulation and Prediction of Swash Oscillations on a Steep Beach. *Coastal Engineering,* 36, pp. 219-242.

Benazir, Triatmadja, R., Rahardjo, A. P. & Yuwono, N., 2016a. *Tsunami Run-up on Sloping Beach based on Dam Break System*. Bali, The 5th International Seminar of HATHI, 29-31 July 2016, pp. 565-574.

Benazir, Triatmadja, R., Rahardjo, A. P. & Yuwono, N., 2016b. *Modeling of Tsunami Run-up onto* Sloping *Beach and its Interaction with Low Structure*. Yogyakarta, The 4th International Conference on Sustainable Built Environment (ICSBE), 12-14 October 2016, pp. 622-630.

Chanson, H., 2005. *Applications of Saint-Venant Equations and Method of Characteristic to the Dam Break Wave Problem,* Brisbane, Australia: Report CH55/05, Departement of Civil Engineering The University of Queensland.

Chanson, H., 2006. Tsunami Surges on Dry Coastal Plains: Application of Dam Break Wave Equations. *Coastal Engineering Journal,* 48(4), pp. 355-370.

Freeman, J. C., and Le Mehaute B., 1964. Wave Breakers on a Beach and Surges on a Dry Bed, *J.* Hydraulic *Div. Am. Soc. Civil Engrs*., 90, pp. 187-216.

Goto, C., Ogawa, Y., Shuto, N. & Imamura, F., 1997. *Numerical Method of Tsunami Simulation with Leap-Frog Scheme,* IOC Manual: IUGG/IOC Time Project, UNESCO.

Hall, J. V. & Watt, G. W., 1953. *Laboratory Investigation of The Vertical Rise of Solitary Wave on Impermeable Slopes,* Washington DC: Army Coastal Engineering Research Centre, Tech Memo 33.

Hibberd, S. & Peregrine, D. H., 1979. Surf and Run-up on a Beach: A Uniform Bore. *Fluid* Mechanics*,* 95(Part 2), pp. 323-345.

Imamura, F., Yalciner, A. C. & Ozyurt, G., 2006. *Tsunami Modelling Manual (TUNAMI Model)*. Sendai: Disaster Control Research Center, Tohoku University.

Kaplan, K., 1955. *Generalized Laboratory Study of Tsunami Run-up*, US Army Corps of Engineers, Tech Memo, 60.

Kuswandi, Triatmadja, R. & Istiarto, 2017. Simulation of Scouring around a Vertical Cylinder due to Tsunami. *Science of Tsunami Hazards,* 36(2), pp. 59-69.

Li, Y. & Raichlen, F., 2003. Energy Balance Model for Breaking Solitary Wave Runup. *Journal of Waterway, Port, Coastal, Ocean Engineering,* 129, pp. 47-59.

Liu, P. L. -F., Synolakis, C. E. & Yeh, H. H., 1991. Report on the International Workshop on Long-Wave Run-up. *J. Fluid Mech.,* 229, pp. 675-688.

Lukkunaprasit, P., Ruangrassamee, A. & Thanasisathit, N., 2009. Tsunami Loading on Building with Opening. *Science of Tsunami Hazard,* 28(5), pp. 303-310.

Miller, R. L., 1968. Experimental Determination of Run-up of Undular and Fully Developed Bore. *Journal of Geophysical Research,* 77(14), pp. 4497-4510.

Packwood, A. R. & Peregrine, D. H., 1981. *Surf and Runup on beaches: Models of Viscous Effects,* England: Rep. AM-81-07, University of Bristol.

Shen, M. C. & Meyer, R. E., 1963. Climb of a Bore on a Beach (Part 3: Run-up). *Fluid Mechanics,* 16, pp. 113-125.

Shuto, N., 1967. Run-up of Long Waves on a Sloping Beach. *Coastal Engineering in Japan*, 10, pp. 23–38.

Shuto, N., 1997. A Natural Warning of Tsunami Arrival. In: H. G., ed. *Perspectives on Tsunami Hazard Reduction.* Dordrecht, The Netherlands: Springer, pp. 157-173.

Synolakis, C. E., 1986. *The Runup of Long Wave.* Ph.D Thesis ed. California: California Institute of Technology.

Synolakis, C. E., 1987. The Runup of Solitary Waves. *Journal of Fluid Mechanics,* 185, pp. 523-545.

Synolakis, C. E., 1991. Tsunami Runup on Steep Slopes: How Good Linear Theory Really Is. Natural *Hazards,* 4, pp. 221-234.

Synolakis, C. E. & Bernard, E. N., 2006. Tsunami Science before and beyond Boxing Day 2004. *Philosophical Transactions of The Royal Society A,* 364, pp. 2231-2265.

Tadepalli, S. & Synolakis, C. E., 1994. The Run-Up of N-Waves on Sloping Beaches. *Proc. R. Soc. Lond. A,* 445, pp. 99-112.

Tadepalli, S. & Synolakis, C. E., 1996. Model for The Leading Waves of Tsunami. *Physical Review Letters,* 77(10), pp. 2141-2144.

Triatmadja, R., 2010. *Tsunami, Kejadian, Penjalaran, Daya Rusak, dan Mitigasinya.* Yogyakarta: Gadjah Mada University Press.

Triatmadja, R. & Benazir, 2014. Simulation of Tsunami Force on Rows of Buildings In Aceh Region After Tsunami Disaster In 2004. *Science of Tsunami Hazard,* 33(3), pp. 156-169.

Triatmadja, R. & Nurhasanah, A., 2012. Tsunami Force on Buildings with Openings and Protection. *Journal of Earthquake and Tsunami,* 6(4), pp. 1-17.

Togashi, H., 1981. *Study on Tsunami Run-up and Countermeasure.* Ph.D Thesis, Tohoku University.

Yeh, H. H., 1991. Tsunami Bore Runup. *Natural Hazard,* 4, pp. 209-220.

Yeh, H. H. & Ghazali, A., 1986. *Nearshore Behavior of Bore on a Uniformly Sloping Beach.* Taipei, Proc. 20th Cmf. Coastal Engineering, pp. 877-888.

Yeh, H. H., Ghazali, A. & Marton, I., 1989. Experimental Study of Bore Runup. *Fluid Mechanics,* 206, pp. 563-578.

Zelt, J. A., 1991. The Run-up of Nonbreaking and Breaking Solitary Waves. *Coastal Engineering,* 15, pp. 205-246.

Zhao, X. L., Wang, B. & Liu, H., 2012. Characteristics of Tsunami Motion and Energy Budget During Runup and Rundown Processes over a Plane Beach. *Physics of Fluids,* Volume 24.

ISSN 8755-6839

SCIENCE OF **TSUNAMI HAZARDS**

Journal of Tsunami Society International

Volume 38 **Number 2** **2019**

ANAK KRAKATAU VOLCANO EMERGENCY TSUNAMI EARLY WARNING SYSTEM

A. Annunziato[1], G. Prasetya[2], S. Husrin[3]

[1]European Commission Joint Research Centre - [2]Tsunami Society Indonesia (IATsI) - [3]Ministry of Marine Affairs and Fisheries of the Republic of Indonesia

ABSTRACT

On 22 Dec 2018 13:56 UTC a tsunami was generated from the area of the Anak Krakatau Volcano, with waves propagating in all directions inside the Sunda Strait - the sea portion between the islands of Java and Sumatra. The cause of this event seems to have a correlation with the ongoing volcanic eruption, which was particularly active since June 2018 [4].

At the time of the event, the Tsunami Early Warning System currently implemented in Indonesia, could not be used because there was no mechanism to activate the system on the basis of sea levels measurements or other information from the volcano activities. Given the situation, the Indonesian authorities decided to implement an Emergency Early Warning System that can timely inform if any sea level disturbance represents a tsunami from volcano activities and therefore be able to activate the warning sirens.

The Joint Research Centre (JRC), in collaboration with the Indonesian Tsunami Society, the Marine Research Centre of the Ministry of Marine Affairs and Fisheries and the Meteorological, Climatological and Geophysical Agency of Indonesia (BMKG) worked together since the event in December in order to design and implement the new Emergency System. The new system will adopt the real time fast Tsunami instruments (Inexpensive Device for Sea Level Monitoring or IDSL), developed by JRC [1], to monitor in real time on a 24/7 the sea level and provide email, SMS alerts, CCTV images and inform about a potential event. The activation of the sirens in the area can be performed after human verification of the signals. The first two devices were

installed at the end of January 2018; other devices will be provided and installed in the near future. The present report illustrates the basic principle of the Early Warning System and reports about the first two months of operational activity since the new devices were installed.

1 THE KRAKATOA TSUNAMI OF 22 DECEMBER 2018

On 22 December 2018 a large tsunami was generated from the collapse of the Krakatau volcano's structure inside the Anak Krakatau Volcanic Complex. The tsunami hit the coasts of Sumatra and Java in the Sunda Strait, with waves up to 6-8 m, causing a huge number of fatalities, currently estimated to be more than four hundred. The tsunami arrived at about 21:30 local time (14:30 UTC) on 22 December, completely unexpected, and caused fatalities and extensive damage along the coastal areas of the Sunda Strait. As of 14 January 2019, there were at least 430 casualties, mostly along the southeast coast of West Java in the Pandeglang Regency (Banten province, Java), 23 people were missing, 7200 were injured, more than 1000 structures were damaged and 430 boats damaged [2]).

At the time of the event, the Early Warning System that had been implemented in Indonesia to protect the people from tsunamis was operational; however, this system had been designed to warn only about tsunamis of seismic origin (which are the majority in the world)[3]. The generation of the tsunami of 22 December 2018 was detected by the tide gauges that had been installed on the coast, but not in sufficient time to provide any warning to the population, about any larger seismic event or the relevant increase in volcanic activity of the Krakatau volcano. In any case the distance from the volcano to coastal areas is rather large to prevent a detailed visual or acoustic alerting. In principle, the availability of the tide gauges datum in real time, connected with an analysis and change detection software, could have allowed to identify the first impulse in Marina Jambu.[1]

Tide Gauge	**Arrival Time on 22 Dec (UTC)**	**Time Difference (min)**	**Max Height (above tide, m)**
Estimated Time of the event	13:58	0	-
Marina Jambu	14:27	29	0.90
Ciwabdan	14:33	35	0.35
Kota Agung	14:35	37	0.36
Panjang	14:53	55	0.28
Bengkunat	16:20	142	0.20
Krui	Not detected		
Binuangen	Not detected		

Tab I – Arrival time at tide gauges and max height

[1] http://tides.big.go.id:8888/dash/prov/Banten.html

Taking into account that 5-8 min of latency are present in the data, there are still many locations not yet reached after 29+8 (latency) = 37 min

In order to have an alert from the sea level change several intermediate steps are necessary:

1. Accurate sea level measurement, as close as possible to the tsunami source
2. Fast data transmission from the measurement location
3. Software to analyse in real time and detect level changes, providing an alert
4. A double check of the data (i.e. CCTV images)
5. Decision to issue an alert to coastal locations
6. Activation of siren systems

Any time delay from 1 to 6 min will reduce the effectiveness of the alerting because when the wave arrives nothing can be done any more.

Given the fact that the Krakatau volcano eruption is still ongoing and at any time a further tsunami event is possible, an emergency implementation of an Early Warning System is of paramount importance in terms of timeliness. A more stable solution can be identified in the next months but something to correct the situation is necessary as a matter of urgency.

The objective of this report, jointly elaborated by the Joint Research Center and Tsunami Research Center Indonesia, is to outline an Emergency System that can help the Indonesian Government to face the immediate situation; future improvements and stable infrastructure can be designed in the future.

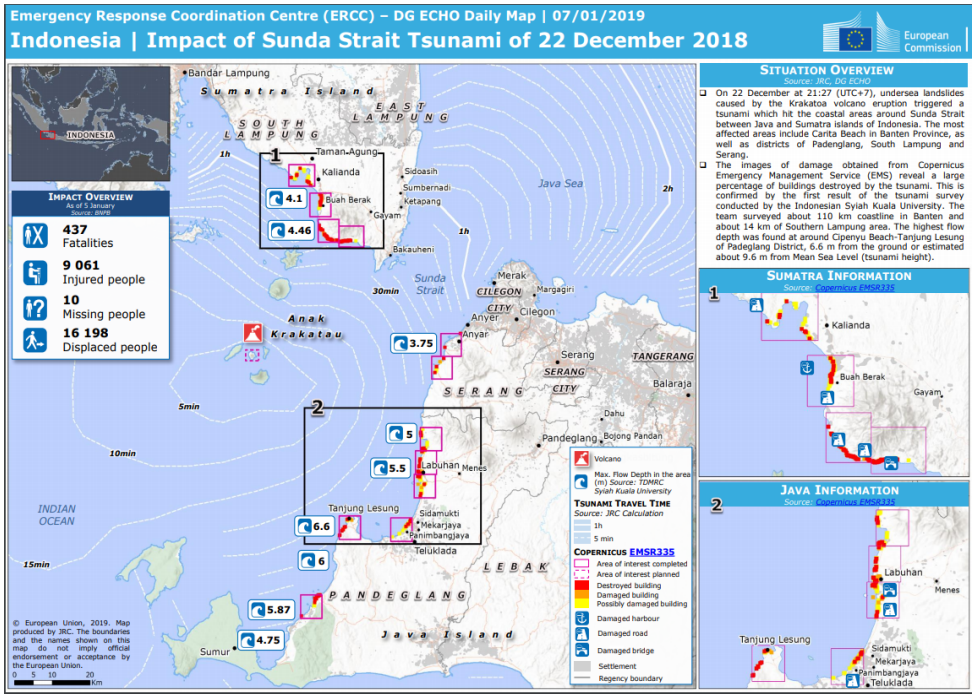

Figure 1 - Impact from the Tsunami caused by the collapse of Krakatoa Volcano

2 TSUNAMI PROPAGATION CALCULATIONS

Taking into account the worse case scenario of the potential tsunami generation by Anak Krakatau with diameter of the Volcano being 2km x 2km, the computation of tsunami propagation and the resulting wave height along the coast is illustrated in Figure 2.

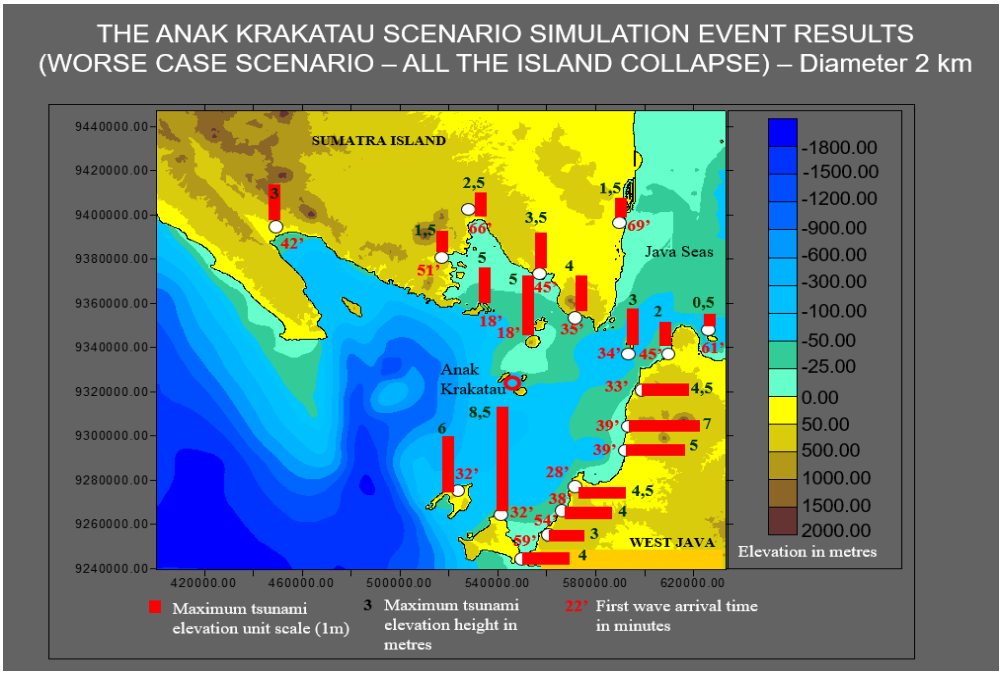

Figure 2 - Travel time (red numbers) and maximum Tsunami height in m (black numbers)

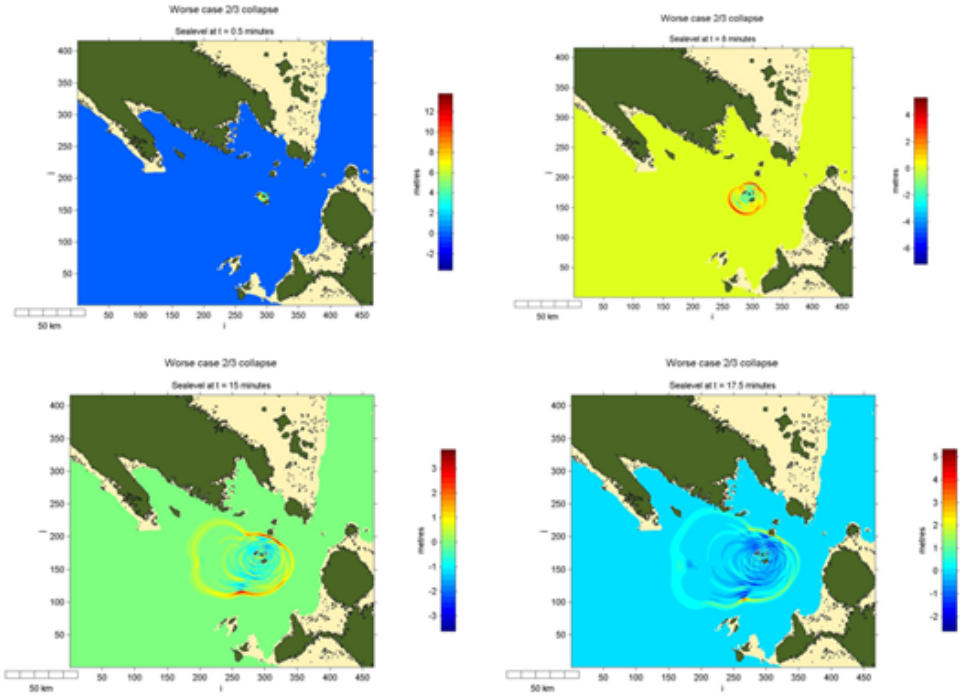

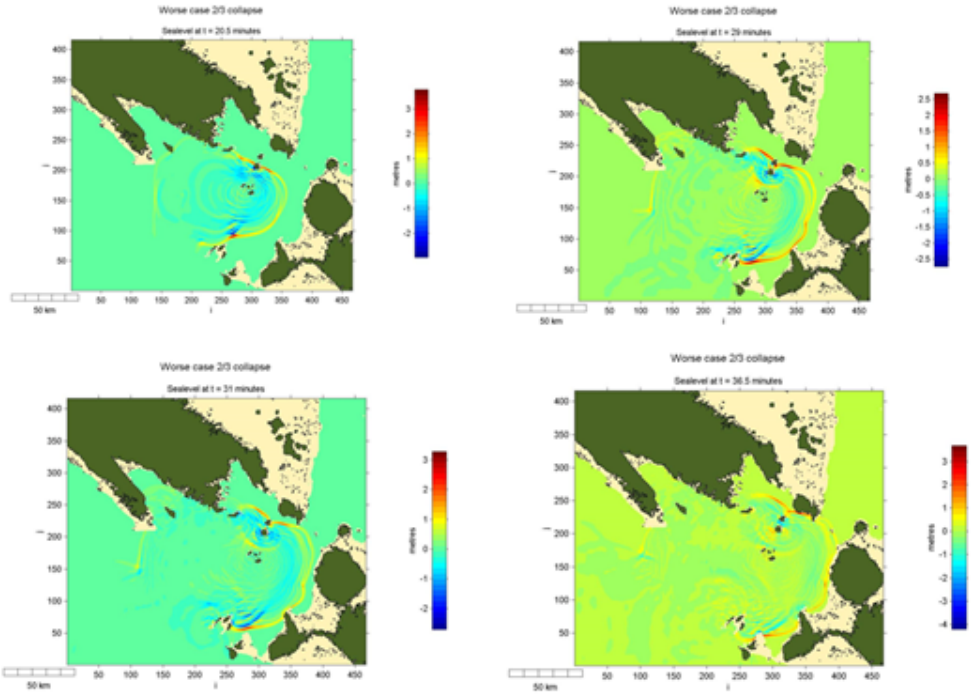

Figure 3 - Wave propagation in the Sunda Strait

3 EARLY WARNING SYSTEM DESIGN

In this section, the current Tsunami Warning System implemented in Indonesia is briefly described. Then an emergency TWS, specifically designed to protect the people from another tsunami generated by the Anak Krakatau volcano is outlined. The definite final system is subsequently described briefly.

3.1 Definition of the new Emergency EWS for the Sunda Strait

The objective is the implementation, in very short time (1 month), of an additional system that can support the operation of the National System until a final dedicated Warning System for the Krakatau volcano is implemented.

The working mode of the emergency system is based on a number of fast response tide gauges, transmitting the sea level in 'almost real time' and having a software on board (or with an analysis system in the collection server), that analyses the sea level and determines if an alert is needed. The coincidence of two or three sea level alerts can be considered as a reliable alert and

- can automatically activate the sirens in the Sunda Strait or
- can issue email/SMS to a list of addresses and someone should then decide to activate the sirens

The second case is the most conservative to avoid false alerts but some time is then lost in order to understand what is happening. Therefore the availability of tide gauges as close as possible (in terms of travel time) to the origin of the waves, is necessary.

Taking into account the travel time determined above, the following solution is proposed:

- Management of the data from the existing instrumentation with the implementation of wave detection and alerting routines.
- Installation of IDSL devices[2] in port areas around the volcano, as much as possible at shortest travel time, with minimum data latency of few seconds.
- Installation of tide gauges on the three islands close to the Anak Krakatau volcano: Sertung, Panjang and Rakata islands, travel time <2 min, alert time 3 min from the event

It is clear that the last set of tide gauges is certainly more useful for the purpose of quick alerting. The remote installation site and the absence of coastal protection for those devices, makes them rather fragile and possibly not always available in case of need. The IDSL devices, designed to provide fast data collection and dissemination, as well as identification of anomalous waves, can constitute a reliable backup or confirmation solution.

[2] Inexpensive Device for Sea Level measurements – IDSL

4 PROPOSED IMPLEMENTATION

The implementation proposed foresees analytical intervention to the existing instrumentation and installation of new fast reacting and fast transmitting instruments (IDSLs)

4.1 Existing instrumentation

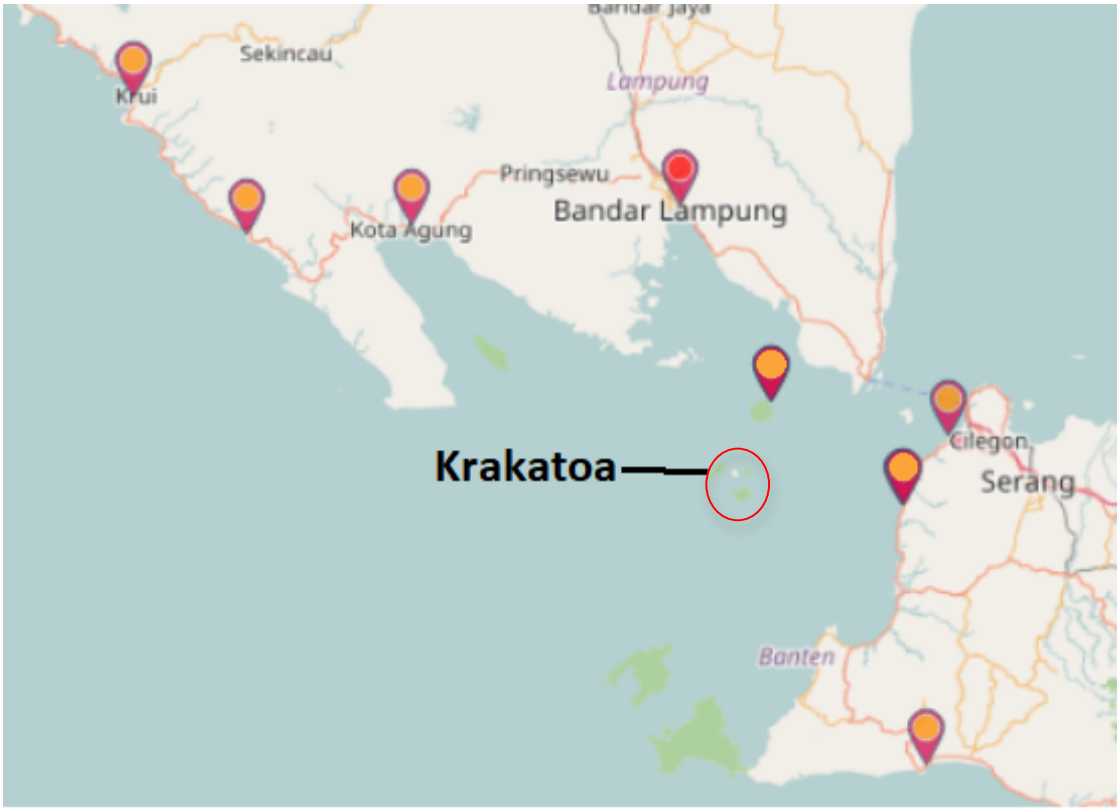

Figure 4 - Existing tide gauges in the Sunda Strait

The existing tide gauges in the Sunda strait are shown in the above figure. The gauges are operated by the Badan Informasi Geospasial (BIG) Institute. The data are collected every 2 or 3 minutes and are made available on the BIG web site. Those data are acquired and included in the TAD server for further processing and formulation of the alert signals (see Appendix A). Unfortunately the latency is rather long (about 10 min) and therefore the signal can take up to 12-14 minutes between measurement and processing, which makes the alerting too delayed. For this reason it is necessary to adopt faster instrumentation (IDSLs). It should be noted that the BIG tide gauge in Sebesi Island was installed on 26 Jan 2019 and therefore was not available at the time of the event.

4.2 Medium Distance Instruments

4.2.1 Possible installation sites

A proper installation site for the IDSL requires a port structure where to fix the pole. Locations close to the port entrance are preferable. In normal conditions it is better to perform a survey onsite in order to define the right position of the instrument, verify the GSM connection and take contacts with local authorities. In this case there is no time to perform all these steps and therefore we will identify the possible installation places from satellite images (Google Earth) and preliminary contacts should be taken with local authorities to be sure that when the installation has to be performed all goes smoothly. The list below is a not exhaustive list of possible locations. A more detailed analysis in collaboration with Indonesia authorities is necessary in order to check whether the locations are possible and if not, if some locations could not be improved with necessary infrastructure to install a tide gauge. We concentrated more on Sumatra, respect to Java as the arrival times here are shorter; also however because in Sumatra many more potential locations are available.

	Location	Lat	Lon	Travel Time (min)	Device present	Notes
Lampung (SUMATRA)						
	Kota Agung	104.621	-5.52338	37	YES	
	Bandar Lampung	105.2865	-5.45358	55	YES	
	Px06	104.5426402	-5.538199375	40		
	Tarahan	105.3654596	-5.557232192	56		Small fisherman port
	Industrial	105.3827018	-5.59305023	53		Industrial dock
	Kalianda	105.5883822	-5.741851675	39		Large Marina **
	P12	105.6122501	-5.833707747	34		Small dock
	P13	105.6472288	-5.836579004	37		Small fisherman port
	Bakahheni	105.7524992	-5.872764	38		Large industrial port
	Px15	105.2278809	-5.587868168	49		Small marina
	Px16	105.1906576	-5.588327294	54		Small dock
	Px17	105.17204	-5.609379404	55		Small dock
2	Px18	105.2205098	-5.732823134	28		Small dock
	Legundi	105.292515	-5.80172512	n.a.		Small dock
1	Siuntjal	105.317415	-5.795647179	27.5		Small dock
	Putih	104.8752156	-5.655967117	32		Long dock, not sure if

						floating
	Px22	104.7268941	-5.554785442	32		small dock
Banten (JAVA)						
	Marina Jambu (O)	105.8346	-6.18963	29		
4	Marina Jambu	105.8395384	-6.189708674	32	YES	
	Ciwandan	105.9437	-6.01444	35	YES	
3	Anier Kidu	105.884252	-6.069176	31		
	Px25	105.8359229	-6.315025722	35		
	Px26	105.819007	-6.359434186	36		
	Kaduperasi (?)	105.8181349	-6.398484035	38		Dock ?
	Px27	105.846862	-6.170636673	36		
	Sebesi2	105.507854	-5.962299	18		Wood dock, suitable ?
	Sebesi Port	105.512787	-5.935818	20	YES	Installed 26 Jan 2019

In the list of locations, considering the arrival time, the 4 best installation sites are

- **Sebesi Port** (at the time of the design of the system no tide gauge was present. A tide gauge was installed on 26 Jan 2019)
- Siuncal
- Px18
- Anyer Kidul
- **Marina Jambu** (device exists at this location)

As it can be seen from the map below, even if 27 min is rather short, leaving short evacuation time, several locations are not yet reached by the wave and will be reached several minutes after. In the figure below in red the coastal locations reached by the wave before 30 minutes. Which means that **a large portion of the coast is not reached yet by the wave.**

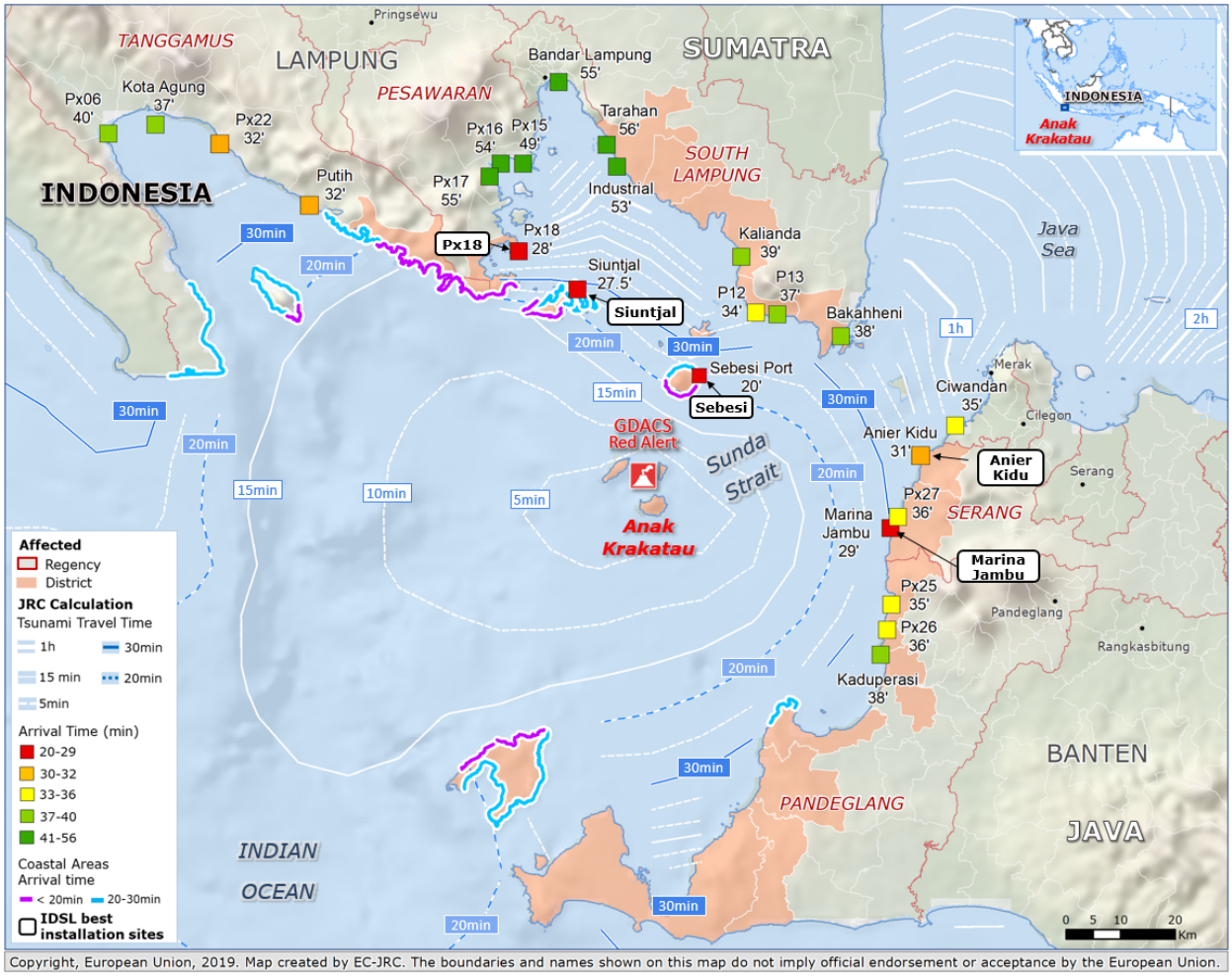

Figure 5 - Arrival Time in minutes in the selected locations for IDSL installation. The coastal locations in violet are reached by the wave within 20 min, the locations in cyan between 20 and 30 min. All the other locations are reached after 30 minutes

If the short term instrumentation is available, practically the whole coastal areas can be alerted if proper siren system is actuated.

However it is important to note that, in case the short distance instrumentation is not available:

- The detection of the alert may occur at about 27 min plus 2-3 min to give the operators the time to verify that it is not a false alert
- It is important to verify the alerting conditions in at least 2 devices, in order to avoid a spike from one device
- That given 30 min as alerting limit, there are still several locations that are reached after 30 min and that, with proper siren alerting can be informed of the incoming wave
- That very strict Standard Operating Procedures (SOPs) are necessary to avoid to lose vital time

4.2.2 Performed Installations

Two installations have been performed at end of January 2019: Sebesi and Marina Jambu; other will be performed in the near future.

4.2.2.1 Sebesi Island

Figure 6 - Location of the Jetty on Sebesi island

The Sebesi island is located about 18 km (center to center) from the Anak Krakatau volcano, and is NNE respect to the volcano. In the opposite site of the volcano, a 130 m long jetty is present that allows medium ferry boats to serve the island needs (tourists and residents). The island has been evacuated after the Tsunami but at the time of the IDSL installation all appeared returned to its original status.

From Wikipedia:

Sebesi *(also Sebeezee, or 'Bleezie') is an Indonesian island in the Sunda Strait, between Java and Sumatra, and part of the province of Lampung. It rises to a height of 844 metres (2,769 ft) and lies about 12 kilometres (7.5 mi) north of the Krakatoa Archipelago; it is the closest large island to Krakatoa, about the same area and height as the remmant of Rakata. Like Krakatoa, it too is volcanic, although there are no dated eruptions known. (A single report of an eruption in*

1680 seems to be a confusion with the Krakatoa eruption reported from that year.) Unlike the Krakatoa Archipelago, Sebesi has permanent streams and is inhabited. Sebesi was devastated during the 1883 volcanic eruption of Krakatoa. Official records give approximately 3,000 people killed, with 1,000 of these being 'non-residents'. By 1890, Sebesi was being re-cleared. It is believed that since it lies closer to Sumatra, it has served as a 'stepping stone' for much of the flora and fauna which was re-established at Krakatoa. By the 1920s, settlers had returned, and today Sebesi is virtually completely cultivated, with only a small area at the peak and some mangrove swamps still natural.

Figure 7 - The preparation of the installation of the IDSL in Sebesi island, followed by several local people

Figure 8 – On the left the BIG tide gauge installation and on the right the IDSL one, both on the Sebesi Port.

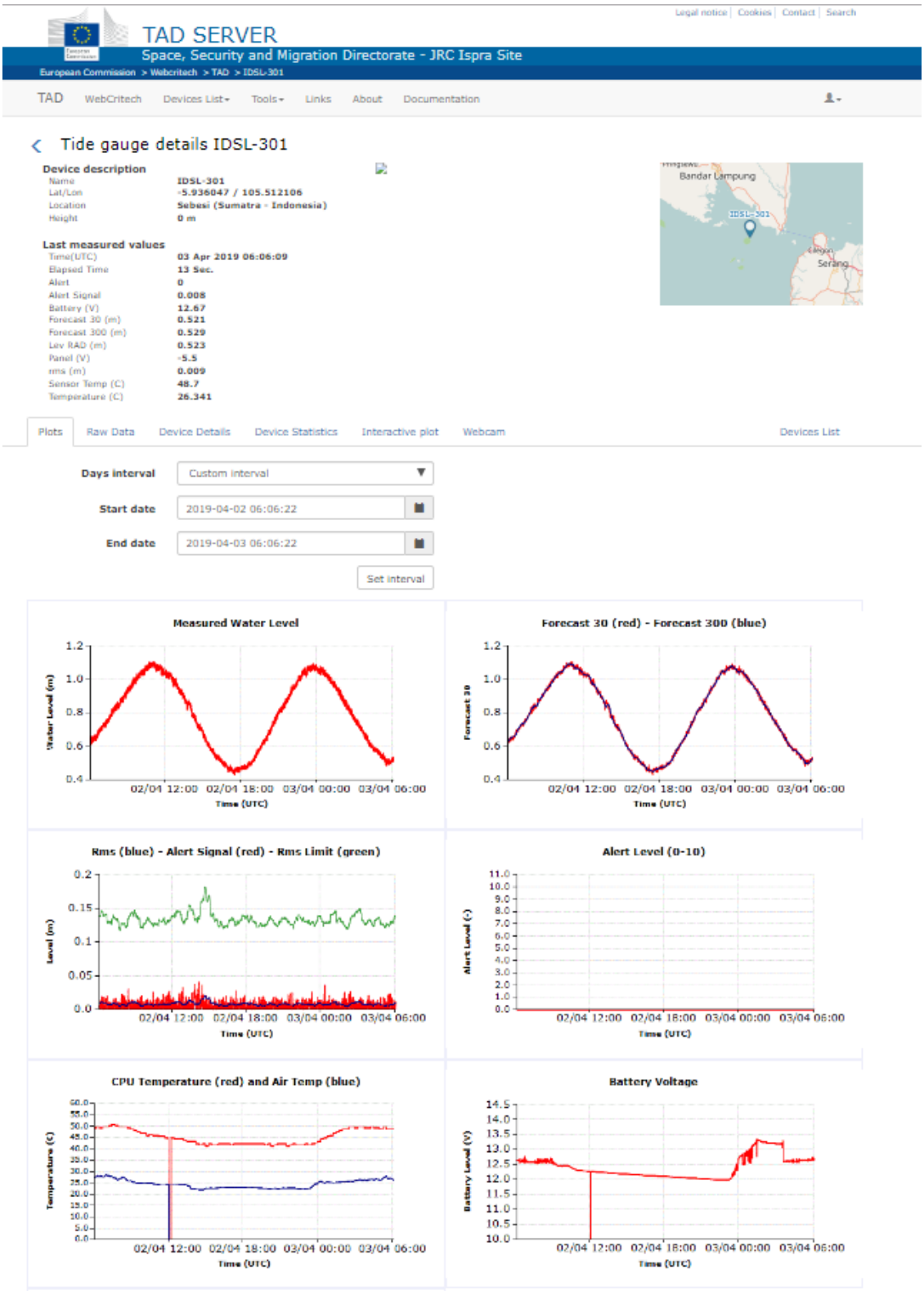

Figure 9 –The web page in the TAD server with the data from Sebesi, *http://webcritech.jrc.ec.europa.eu/TAD_server/Device/206*

The installation in Sebesi was performed on 30th Jan 2019 and since then is transmitting 1 point every 6 seconds, with 5-10 s of latency. There was a period (3-15 March) of data missing due to a problem in the GSM Telecom contract, then solved. Unfortunately the webcam installed on the IDSL does not work, probably damaged during the transport on site; it will be replaced soon.

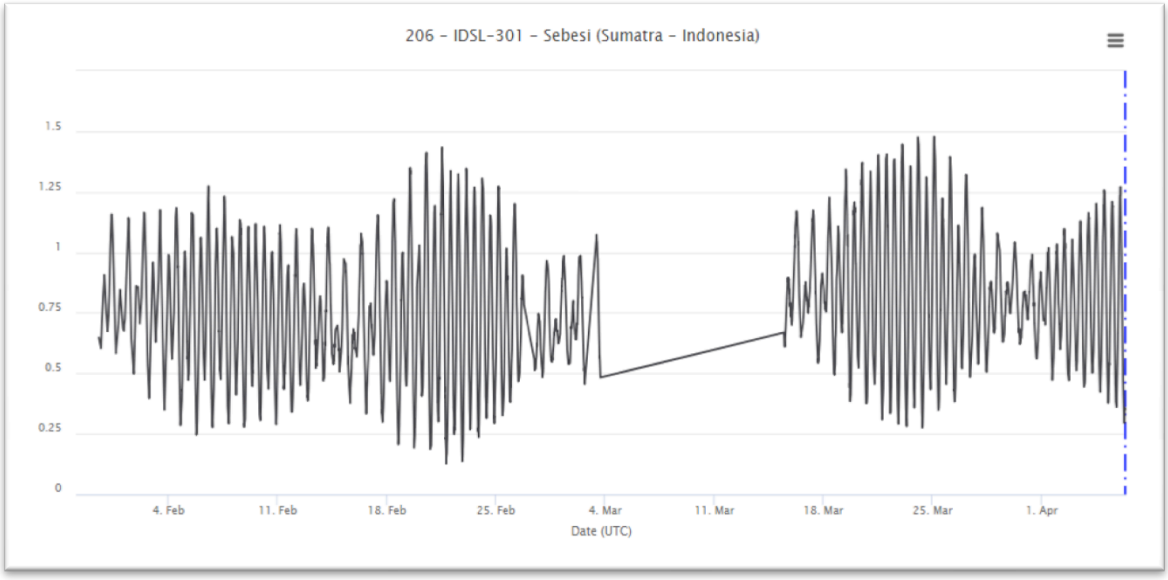

Figure 10 –The whole dataset for Sebesi Island. It is possible to note the data missing between 3 and 15 March, after which the telecom contract has been restored.

4.2.2.2 Marina Jambu

The installation in Marina Jambu was performed on 29th Jan 2019 at a location close to the existing tide gauge from BIG. In this way it is possible to compare the two instrument behaviour. Marina Jambu is one of the main ports in the Sunda Strait and it contains the tide gauge of BIG that detected as first the Tsunami of 22nd Dec 2018.

The IDSL device was positioned close to the existing BIG device, and also at this device the webcam was installed, working correctly since the time of the installation. The webcam provides very clear image of the state of the sea every 15 min; in case of a detected wave, the time interval reduces to 2 min.

The installation in Sebesi was performed on 29th Jan 2019 and since then is transmitting 1 point every 6 seconds, with 5-10 s of latency.

Figure 11 - The Marina Jambu tide gauge is in the center, the red building, before the installation of the IDSL.

Figure 12 – On the left the BIG installation, on the right the IDSL device in Marina Jambu.

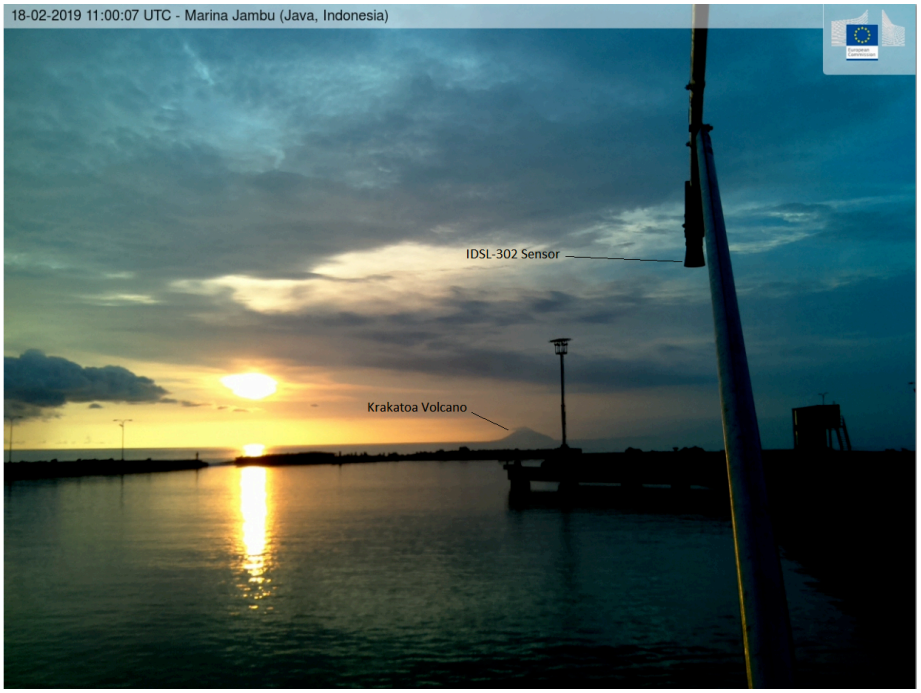

Figure 13 – The image from the webcam shows the IDSL sensor and on the back the Krakatoa complex. The webcam collects one image every 15 min and during detected events, every 2 min.

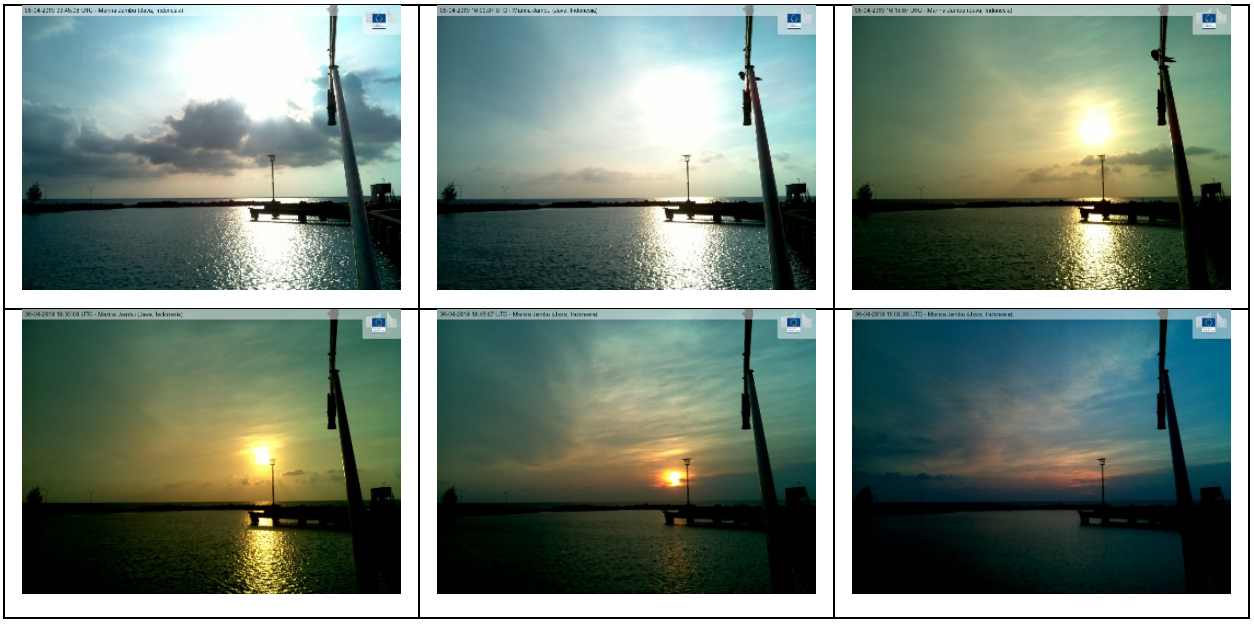

Figure 14 – A sequence of images every 15 min (6 April 2019). All the images are accessible from the TAD_server web site and can be seen as a sequence.

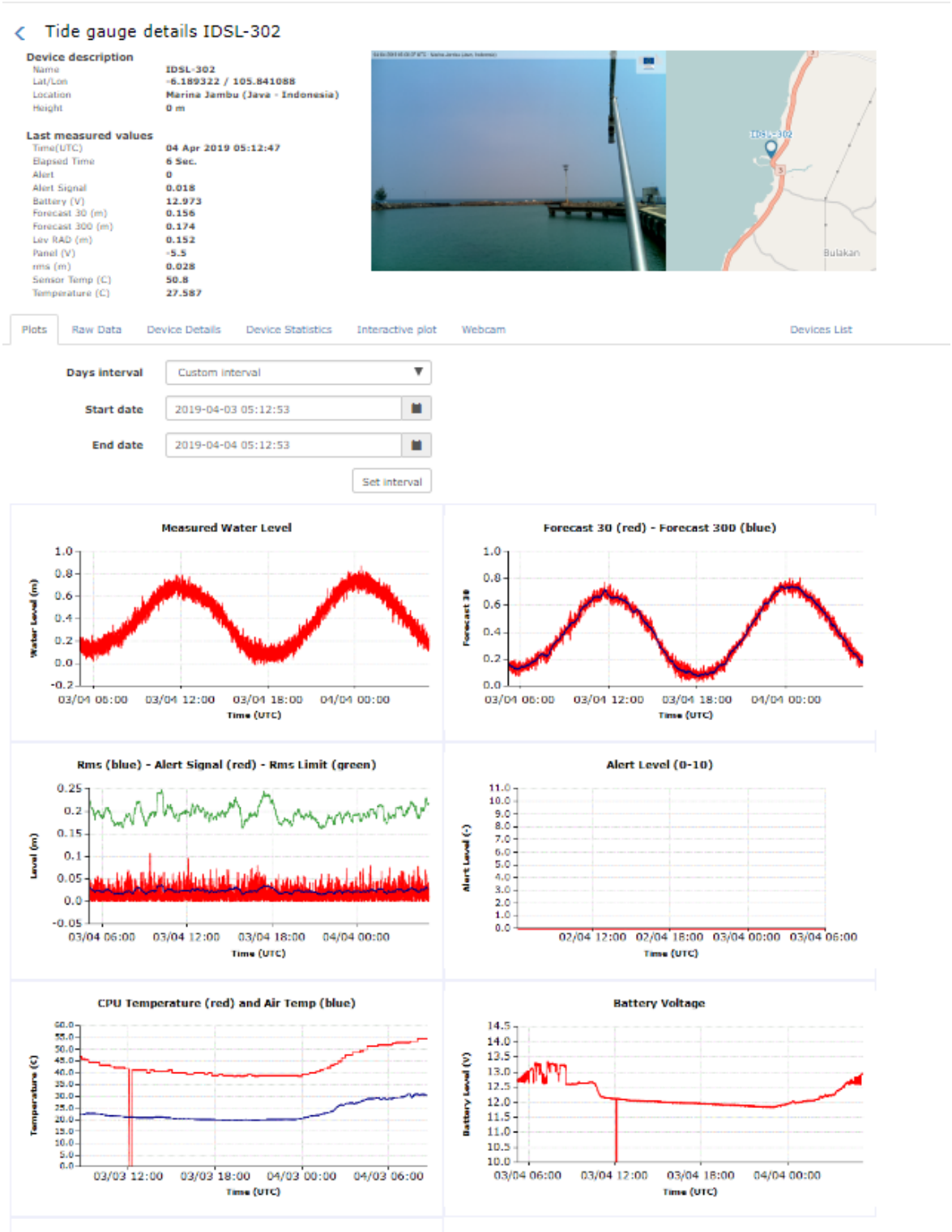

Figure 15 – The web page in the TAD server with the data from Marina Jambu, *http://webcritech.jrc.ec.europa.eu/TAD_server/Device/207*

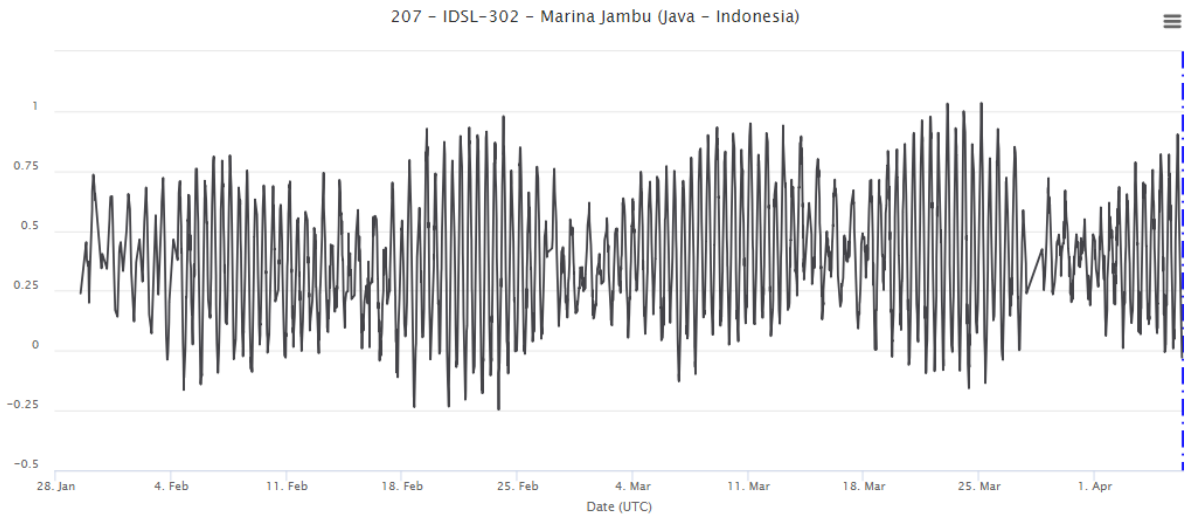

Figure 16 - The whole dataset from the installation to current date

4.3 Short Distance instruments

Figure 17 - the 3 islands around the Anak Krakatau volcano; the arrow indicates the possible installation site, once the communication problems are solved

The installation of instruments on the three islands around the Anak Krakatau volcano would guarantee a minimum time for the arrival time and therefore would leave more time for the alerting. A survey around the island allowed to identify a possible platform for installation south of Krakatua island. However there is not GSM coverage on the islands (17 km from the closest inhabited island) and therefore UHF or satellite communication is necessary in order to have online data availability. Discussion are under way with Governmental authorities and Telecommunication company to install communication system on one of the 3 islands and thus facilitating the installation of instruments.

5 DATA PROCESSING AND ALERT MECHANISMS

All the data from the existing and the new instrumentation reach a common hub where to store the acquired data and made available to whoever wants to use them: http://webcritech.jrc.ec.europa.eu/TAD_server?group=Indonesia .

Devices List - Indonesia

Id	Name	Sensor	Location	Country	Provider	Last Value	Last Date	Elapsed Time
Indonesia								
191	BIG-001	RAD	ToliToli	Indonesia (Sulawesi)	BIG	6.610	04 Apr 2019 02:35:00	2 Hours
192	BIG-002	RAD	Mamuju	Indonesia (Sulawesi)	BIG	0.370	04 Apr 2019 05:00:00	18 Min.
193	BIG-003	RAD	Pantaolan	Indonesia (Lampung)	BIG	0.560	04 Apr 2019 05:00:00	18 Min.
194	BIG-004	RAD	Kota Agung	Indonesia (Lampung)	BIG	0.870	04 Apr 2019 05:00:00	18 Min.
195	BIG-005	RAD	Krui	Indonesia (Banten)	BIG	0.580	04 Apr 2019 05:00:00	18 Min.
196	BIG-006	RAD	Bengkunat	Indonesia (Banten)	BIG	0.200	04 Apr 2019 05:00:00	18 Min.
197	BIG-007	RAD	Pelabuhan	Indonesia (Banten)	BIG	0.660	04 Apr 2019 05:00:00	18 Min.
201	BIG-008	RAD	Binuangeun	Indonesia (Banten)	BIG	7.970	04 Apr 2019 04:50:00	28 Min.
200	BIG-009	RAD	Ciwandan	Indonesia (Banten)	BIG	1.230	04 Apr 2019 04:50:00	28 Min.
190	BIG-010	RAD	Marina Jambu	Indonesia (Banten)	BIG	0.170	04 Apr 2019 04:50:00	28 Min.
209	BIG-011	RAD	Sebesi	Indonesia (Banten)	BIG	0.600	04 Apr 2019 04:50:00	28 Min.
206	IDSL-301	RAD	Sebesi	Indonesia (Sumatra)	JRC-MMAF	0.520	04 Apr 2019 05:18:26	4 Sec.
207	IDSL-302	RAD	Marina Jambu	Indonesia (Java)	JRC-MMAF	0.185	04 Apr 2019 05:18:17	13 Sec.

Figure 18 – TAD Server list of acquired locations.

In all the instrument data an alert value is computed (on the data logger in the case of IDSL, on the JRC server for the BIG data) using a methodology that computes the difference between the signal and the tide that is estimated with a modified Kalman filter type. When this difference exceeds a number of times the standard deviation of the signal the alert level is incremented of one unit (10 units is the maximum alert level).

When the alert level exceeds 5 units an email and SMS is issued to a list of specified subscribers, including at the moment BMKG and also the Australian Bureau of Meteorology (BOM). The Indonesia BMKG, once getting the alert can eventually activate the downstream alerting component (sirens, messages etc) to inform the population of the ongoing event, after a verification that at least another instrument provided the same response.

When the alert level exceeds 1 unit the webcam is requested to perform an image every 2 min. Detail about the system are included in Appendix B.

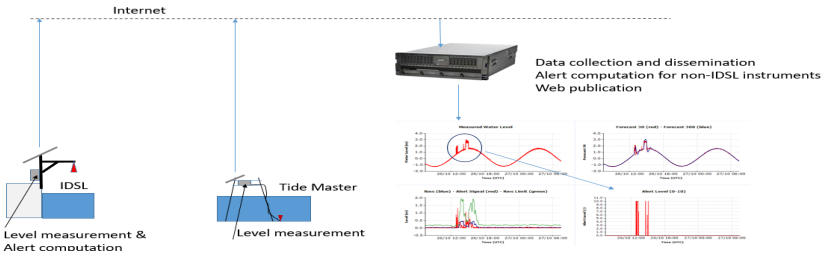

Figure 19 - Data Flow and Processing

An example can be visualized for Ciwandan for the case of 22nd Dec 2018:

http://webcritech.jrc.ec.europa.eu/TAD_server/Device/188?tmin=21%20Dec%202018&tmax=24%20Dec%202018

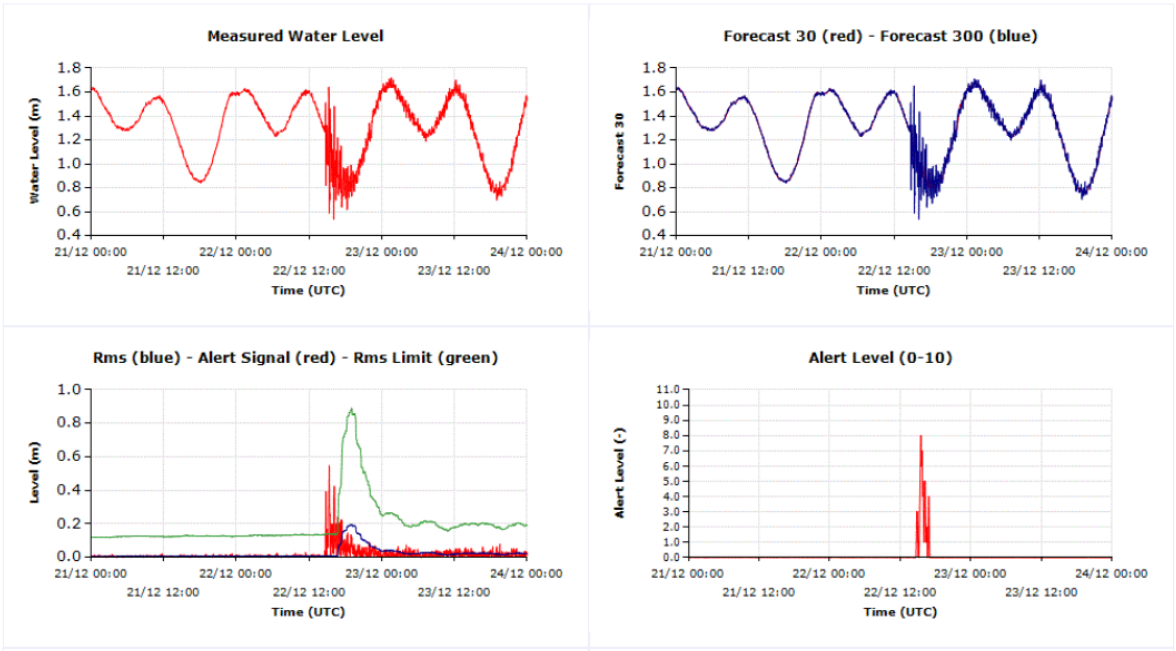

Figure 20 - Algorithm response to the tide gauge signal in Ciwandan on 22 Dec 2018.

From the figure above it is possible to note that the presence of the large oscillation is detected by the system providing an alert of level 8 or 9.

An overview of the current status of the various gauges is also available here:

http://webcritech.jrc.ec.europa.eu/TAD_server/Tools/SensorMonitor/Show/932e3105f5144258abd363f76aac8a01

An example of the comparison between the BIG and IDSL data in Sebesi island in the figure below. It is possible to note the highest acquisition frequency of the IDSL and the shortest latency. The vertical dotted line represents the current time and the last IDSL point is practically coincident with the current time while in the case of BIG data a delay exists.

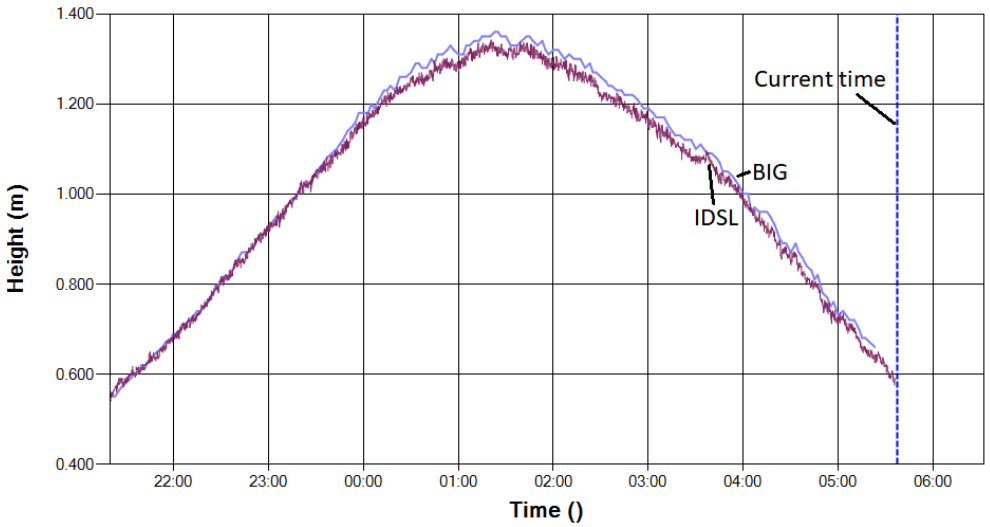

Figure 21 – An example of the comparison between the BIG and IDSL data in Sebesi island. It is possible to note the highest acquisition frequency of the IDSL and the shortest latency

6 CONCLUSIONS

The Sunda Strait Tsunami of 22 Dec 2018, caused by the Anak Krakatau volcano eruption, which struck the Indonesia coasts causing hundreds of fatalities demands for a dedicated effort to setup a proper alerting mechanism for the coastal population.

The report describe a possible solution with the installation of a sea level realtime alerting mechanism based on existing and new tide gauges which are continuously monitored to detect anomalous signals.

The best position for the installation of the new tide gauges has been identified. If realized and the data properly processed, those instruments could provide a long time for alerting, up to 30 minutes. However for the short arrival time locations (within 1-2 min) some concerns for the

installation mode are identified. Two IDSL devices have been installed in January 2019; other six devices will be deployed to Indonesia before summer 2019.

For the medium arrival time locations (20 min to 30 min) the IDSL system will allow to alert a large coastal portion if the alerting signal is taken into consideration and if the siren alerting system is available and provide for most of the coast 10-20 minutes of available time to

REFERENCES

[1] A. Annunziato - THE INEXPENSIVE DEVICE FOR SEA LEVEL MEASUREMENTS - Journal of Tsunami Society International ,Vol. 34, No. 4, page 199 (2015)

[2] BNPB - TSUNAMI SELAT SUNDA (Update 14 Januari 2019), A press release by Pusat data dan Informasi BNPB – Jakarta (2019)

[3] BMKG – TIMELINE TSUNAMI SELAT SUNDA – A press release by Pusat Gempa Bumi dan Tsunami BMKG, 30 Desember 2018 – Jakarta (2018)

[4] ESDM – AKTIVITAS GUNUNG ANAK KRAKATAU 28 DESEMBER 2018 – A press release by Pusat Vulkanologi dan Mitigasi Bencana Geologi ESDM, 29 Desember 2018, Jakarta (2018)

6 APPENDIX A – DESCRIPTION OF IDSL

A new mareograph device has been designed at the Joint Research Centre (JRC) of the European Commission (EC) in order improve the sea level network in use for the Tsunami Hazard monitoring in the Mediterranean Sea and in the North Atlantic area (NEAMTWS area of UNESCO). The instrument has the characteristic to be cheap and very effective but its reliability, duration and quality need to be determined and qualified. For this reason a number of experimental campaigns are being conducted, whose first results are presented here. In collaboration with the UNESCO/IOC (Intergovernmental Oceanographic Commission), responsible of the definition of the Tsunami Warning System of this geographical area, a set of 30 devices have been installed by JRC.

Based on the experience of other similar devices and the need during a Tsunami analysis, the requirements that we have fixed for the mareographs are the following:

- High quality of the data with an error of **0.5 cm** maximum (sensitivity justified by the expected error in the sea level calculations)
- Short acquisition time interval, **5 s** maximum (to have a well-defined sea level wave description over time)
- Small transmission latency, smaller than **15 s** (this is particular important for small basins with low travel time)
- Low overall cost, less than **2.5 k€**
- Autonomy, at least **3 days** without solar irradiation (the autonomy can be increased to 7 days with an over cost and weight on the battery)

The heart of this device is the Raspberry Pi, which is a powerful electronic board that contains a Linux operating system with several standard components (USB, HDMI, Ethernet port, Video card, and sound card) and other busses that can easily be connected with external devices. The device therefore has a computer on which software can be installed and that can be reached remotely for debugging or software change. The other important component is the radar sensor: we have identified a relatively low cost rugged component that could be used as sea level sensor. Additional components are necessary in order to have an autonomous system (electrical power feed and communication). The communication is through the GSM line, which imposes the installation in areas reached by this cellular network. In principle satellite images could also be possible but has not yet tested.

The whole list of IDSL devices can be consulted and the data downloaded at this web site:
http://webcritech.jrc.ec.europa.eu/TAD_server/Home?group=IDSL

Figure A.1 - Typical installation of an IDSL device (Portopalo di Capo Passero, Italy)

APPENDIX B - DESCRIPTION OF TAD SERVER METHODOLOGY

The TAD (Tsunami Alerting Device ®) server has been developed in order to analyse and serve the Tsunami Alerting Panel for which JRC has a patent ongoing. The same system is however used for collecting all the IDSLs and to provide calculations of the alerting parameters to other retrieved data from Internet.

In this case the TAD server will be used both for the IDSLs that will be installed as well as for all the other instruments.

The system is composed of 3 components:

- The data collection and analysis (IDSL software or GaugListener software)
- The data ingestion programme
- The web component for data presentation

Data Collection and Analysis

The method is based on the composition of a URL basic string that is filled with the proper parameters; when the analysis programme is running.

http://webcritech.jrc.ec.europa.eu/TAD_server/EnterData.aspx?idDevice=$IDdevice&log=$S$IDdevice,$DATE,$TIME,$TEMP,$PRESS,$LEV,$FORE30,$FORE300,$RMS,$ALERT_LEVEL,$ALERT_SIGNAL,$V1,$V2,$E

In the case of IDSL the level is read from the sensor. In the GaugeListener the level is acquired via internet from an open data source. In both cases the level is used in order to apply the Change Detection Algorithm (CDA) described below. The CDA provides FORE30, FORE300, RMS, ALERT LEVEL and ALERT SIGNAL parameters that are also composing the storage URL.

The change detection algorithm is based on the estimation at each new data acquisition of the absolute difference between the long term forecast (FORECAST300) and the short term forecast (FORECAST30). The FORECAST300 is the estimation of the value of the current point, performed by calculating the least square 2nd order polynomial related to a long period (1.5-3h of data); the FORECAST30 is the same quantity, estimated using a shorter time (10-20 min). The difference tends therefore to identify sudden changes of the sea level. However for very noisy signals the change could be due to an increase of the noise. Therefore we compare the difference with a number of times the root mean square of the signal in the period of estimation of the FORECAST300. When the difference is positive, the alert level increases of 1 unit; when it comes back below the threshold, the alert level decreases of 1 unit. The maximum value of the alert level is 10.

IF abs(Fore30-Fore300)> rms(time300) then AL=AL+1

In order to avoid that for very smooth and with very small RMS a single spike creates an alert we also introduce a minimum value of the difference; so instead of the rms we use the maximum between rms and a threshold. All these parameters are defined in the configuration file of the devices. Below is an example of the Mamuju device

```
   Example of configuration file for Mamuju device
   title          = Mamuju
   IDdevice       = BIG-002
   serverAddress                                                    =
http://tides.big.go.id:8888/kacrut/0009MMJU02/temp.csv
   ServerPort     = 0
   OutFolder      = .\logs\
   SaveURL=
http://webcritech.jrc.ec.europa.eu/TAD_server/xxxx.aspx?idDevice=
$IDdevice&log=$S$IDdevice,$DATE,$TIME,$TEMP,$PRESS,$LEV,$FORE30,$FORE300,$RMS
,$ALERT_LEVEL,$ALERT_SIGNAL,$V1,$V2,$E
   AlertURL       = none
   DataFile       = logs\Data_yyyyMMdd.txt
   #errLog        = logs\errLog_yyyyMMdd.txt
   Datalog        = logs\dataLog_yyyyMMdd.txt
   Interval       = -1
   n300           =  100
   n30            =  10
   threshold      = 0.05
   ratioRMS       = 2
   AddRMS         = 0.1
   backFactor     = 0
   vmin           = -2
   vmax           = 10.
   remAndInvert   = 0.
   mode           = DOWNLOAD
   type           = BIG
```

As an example the plots below show the various signals for the Sunda Tsunami case and the measurement in Marina Jambu. It is possible to note that at 14:27 the alert level starts to rise and at 14:45 surpasses the level 5, that is considered an alert level suitable for alerting. *It should be*

noted that the data from those measurements have a very large interval (2-3 min) and since the alert level rises of 1 unit every time that a new estimation is done, with such a large interval it takes "at least" 30 min to go from 0 to 10. In the case of IDSL, with an interval of 5 s between two successive points, the interval is much shorter , 50 seconds.

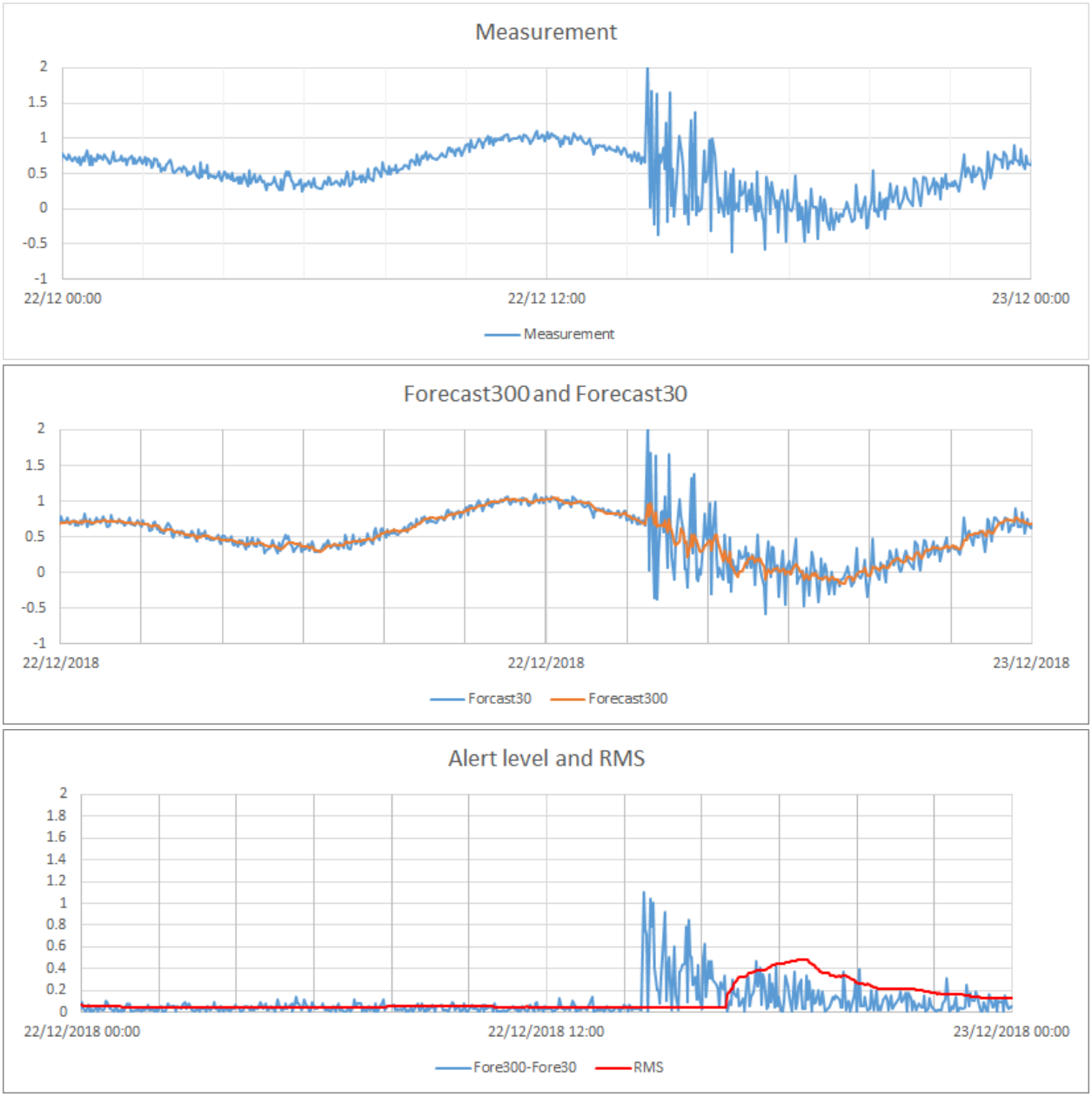

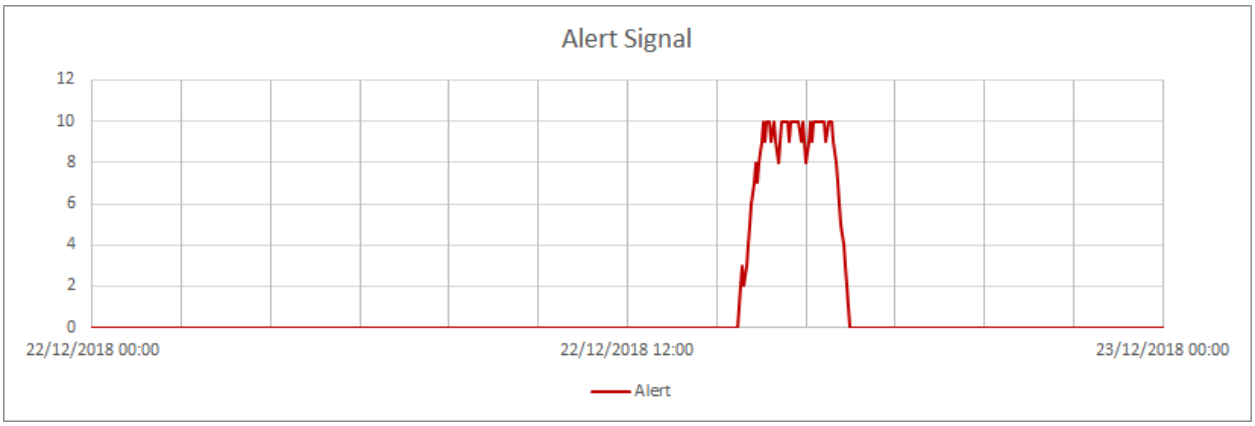

Data Ingestion

Once the data are pushed into the web server with the URL shown above, another programme, continuously running on the server, introduce the data in the SQL server database. The reason for this choice was done in order to prevent an overload of the database. At the beginning it was decided to store immediately the data but we realized that with a huge amount of data the database was not working properly and was slowing down the reply to the IDSLs that therefore were penalized. So we decided to have a separate task that takes the data, stored by the web server in dedicated accumulation files and process them for introduction into the database.

The web component for data presentation

The web site for data presentation is rather standard, showing all the measured and derived quantities and offering the export of all the quantities in various formats for the users.

The web site address URL is: http://webcritech.jrc.ec.europa.eu/TAD_server

ISSN 8755-6839

SCIENCE OF TSUNAMI HAZARDS

Journal of Tsunami Society International

Volume 38 Number 2 2019

LONGTERM COMPARATIVE STUDY OF GROUNDWATER QUALITY IN TSUNAMI AFFECTED COASTAL AREAS OF SIRKALI REGION OF NAGAPATTINAM DISTRICT, TAMILNADU, INDIA

[1] N. RAVISANKAR [2] N. NAGARAJAN [3] S. POONGOTHAI

[1, 2] Assistant Professor, [3] Professor
Department of Civil Engineering, Faculty of Engineering and Technology
Annamalai University, Annamalainagar, Tamilnadu, India

Email: [1] - ravisankar_natarajamani71@yahoo.in ; [2] - nnrajan.au@gmail.com; [3] - spoong86@yahoo.com

ABSTRACT

Sirkali region is under Nagapattinam district of Tamilnadu, India. The water quality in this region is affected significantly by Tsunami, 2004. Historical data on groundwater quality of observation wells of the study area before Tsunami were collected (1966 – 2012) and groundwater samples after Tsunami were also collected and analyzed for water quality parameters. Spatial analysis of water quality parameters before and after Tsunami was carried out. Various maps were prepared using ILWIS. Results show that there is significant degradation in the water quality due to Tsunami in the study area. Vertical electrical soundings [VES] were conducted in the study area. Based on hydro geological conditions, the approximate depth to freshwater/saltwater interface of Sirkali taluk is 4.489 m.

Keywords: *Tsunami, Ground Water Quality, ILWIS, Vertical Electrical Sounding (VES)*

INTRODUCTION

The study area is the coastal region of Sirkali Taluk, Nagapattinam District, Tamilnadu, India, where the Cauvery deposits its rich silt after meandering several hundreds of kilometers. Sirkali region is surrounded by Bay of Bengal on the east, Kollidam River on the west and north Cauvery River on the south.

It lies in between latitudes of N11º 6’ 00” and N11º 27’ 00” and longitudes in between E79º 36’ 00” and E79º 54’ 00”. It is located in the east coastal region of Bay of Bengal. **Figure 1** shows the location details of the study area. A greater part of region consists of deltaic plains of the Cauvery River with very rich fertile soil. Agriculture is the main stay of rural population. The chief sources of irrigation are canals and tube wells. The water quality in this coastal region is affected significantly by the tsunami of 26 December 2004.

OBJECTIVES OF THE STUDY

The prime objectives of the study are,

- Assessment and monitoring of Groundwater Quality in Tsunami affected coastal tract of Sirkazhi region of Nagapattinam District.
- Delineation of sea water/ fresh water interface by geophysical methods and studying the chemical constituents in the groundwater.

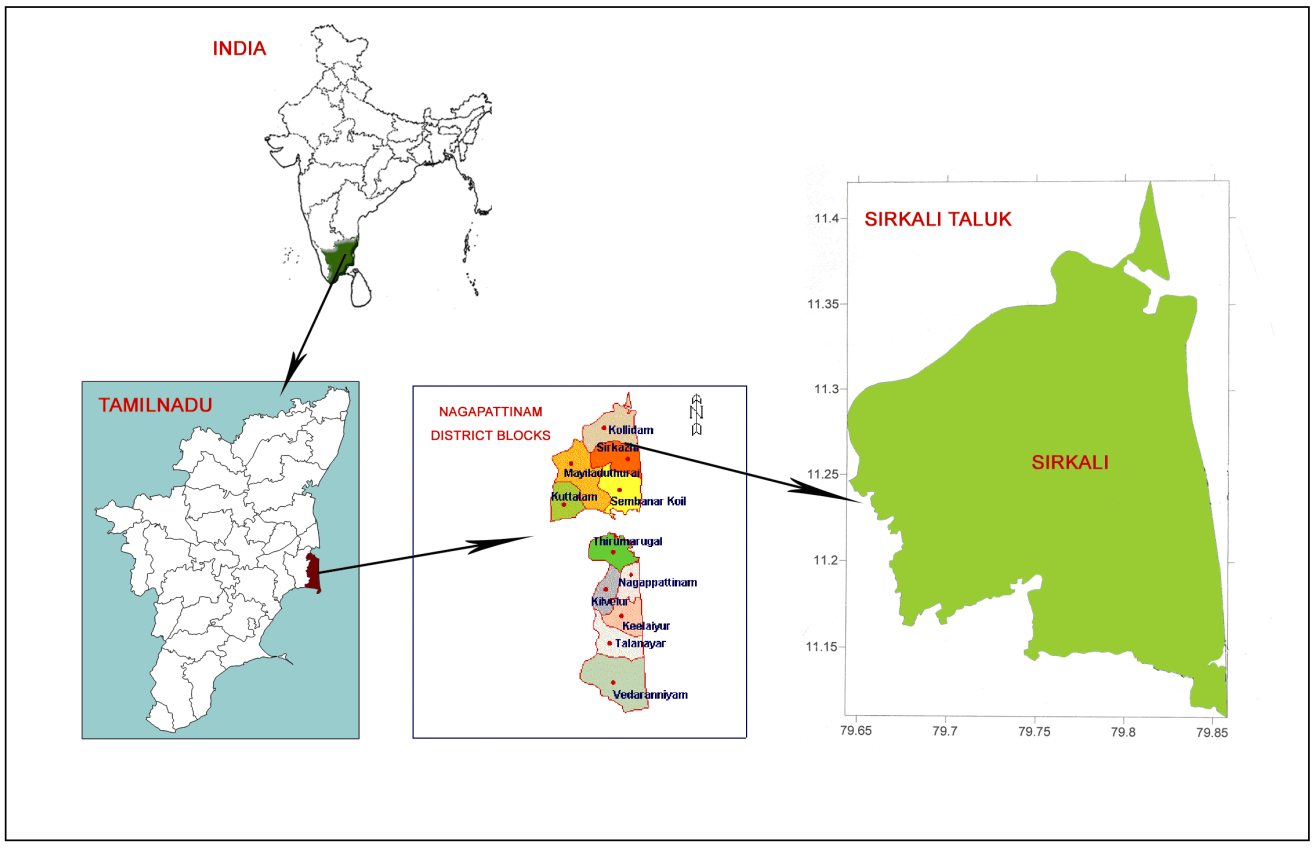

Figure 1 Location and salient features of the study area

MATERIALS AND METHODS

Figure 2 shows the methodology flowchart.

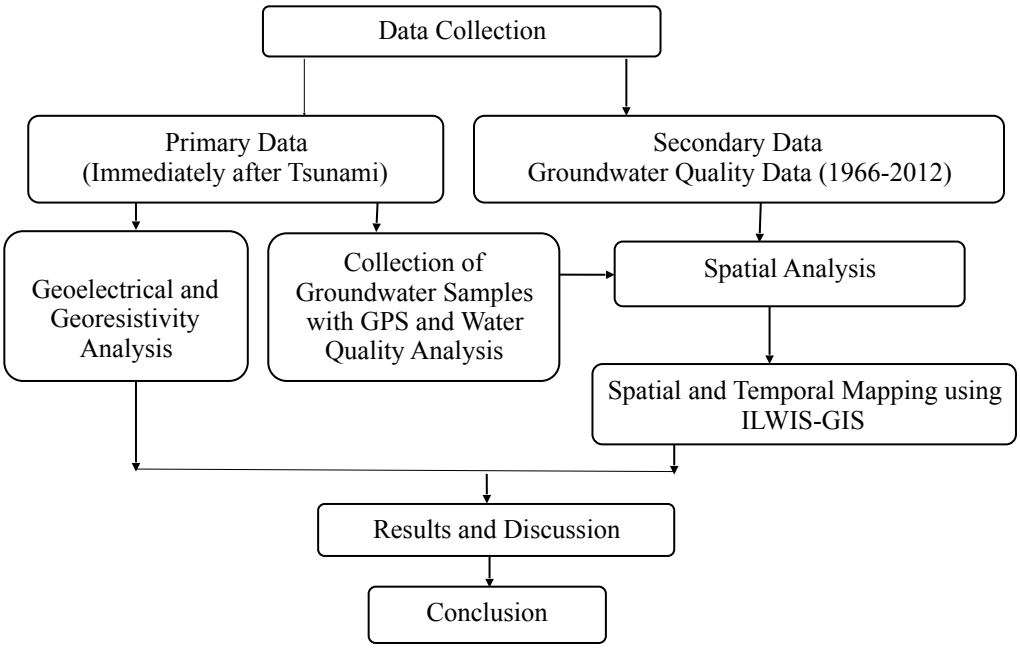

Figure 2 Methodology flow chart.

The methodology of this study depends upon both primary and secondary data. The primary data consists of geochemical, geoelectrical and resistivity data. Collection of groundwater samples during the study period of 2005 to 2012 in Sirkali and Kollidam panchayat unions. The secondary data consists of long - term historical data during the period from 1966 to 2012 on water quality for four observation wells were collected from Groundwater Division, PWD, Tamilnadu. Groundwater quality analysis was carried out in three ways. They are 1. Hydrogeochemistry, 2. Spatial mapping using ILWIS and 3.Correlation analysis.

RESULTS AND DISCUSSIONS

Spatial analysis of various water quality parameters before and after Tsunami was carried out and various maps were prepared using ILWIS – GIS package as shown in **Figure 3** to **Figure 6**. It is observed that the major pollution is due to Cl, EC, pH and Na. Results show that there is significant degradation in the water quality due to Tsunami in the study area. Also a systematic geoelectrical investigation was carried out of the study. Vertical electrical soundings [VES] were conducted in the Tsunami affected villages at the water sampling locations using Microprocessor based signal stacking digital resistivity meter. The depth of investigation is AB/2 – 25 meters. Based on hydro geological conditions, TDS parameters and VES data interpretations, the approximate depth to freshwater/saltwater interface and the subsurface lithology were delineated. This study reveals that the approximate and average depth to freshwater/saltwater interface of Sirkali taluk is 4.489 m.

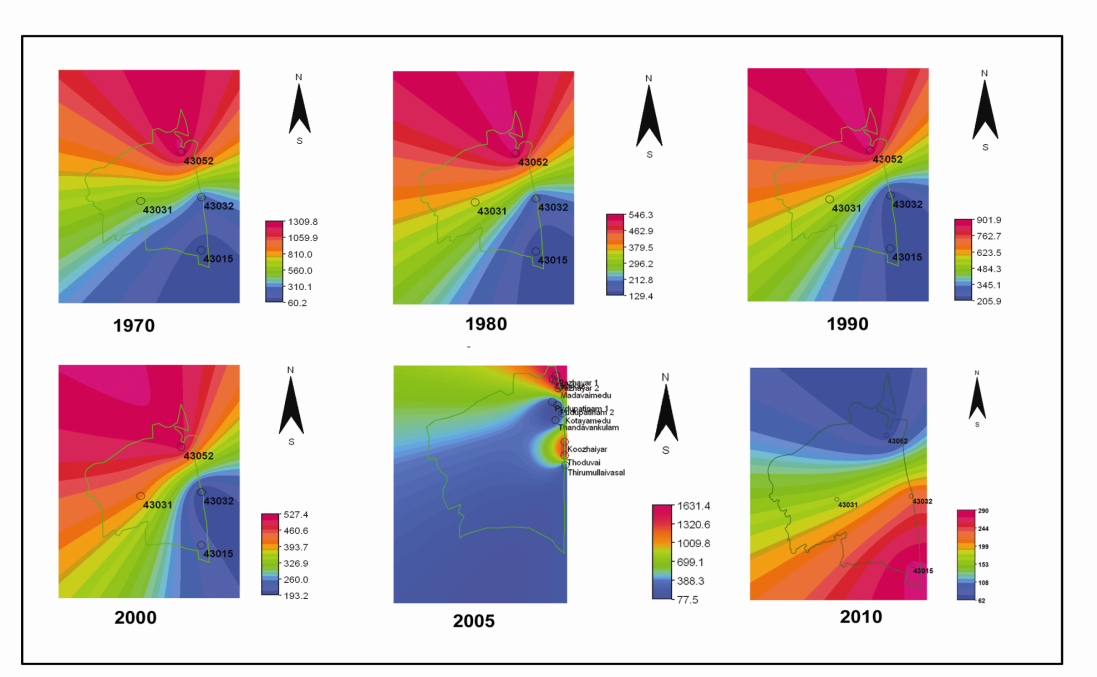

Figure 3 Spatial mapping of Groundwater quality Parameter before and after Tsunami -Cl (mg/L), 1970-2010

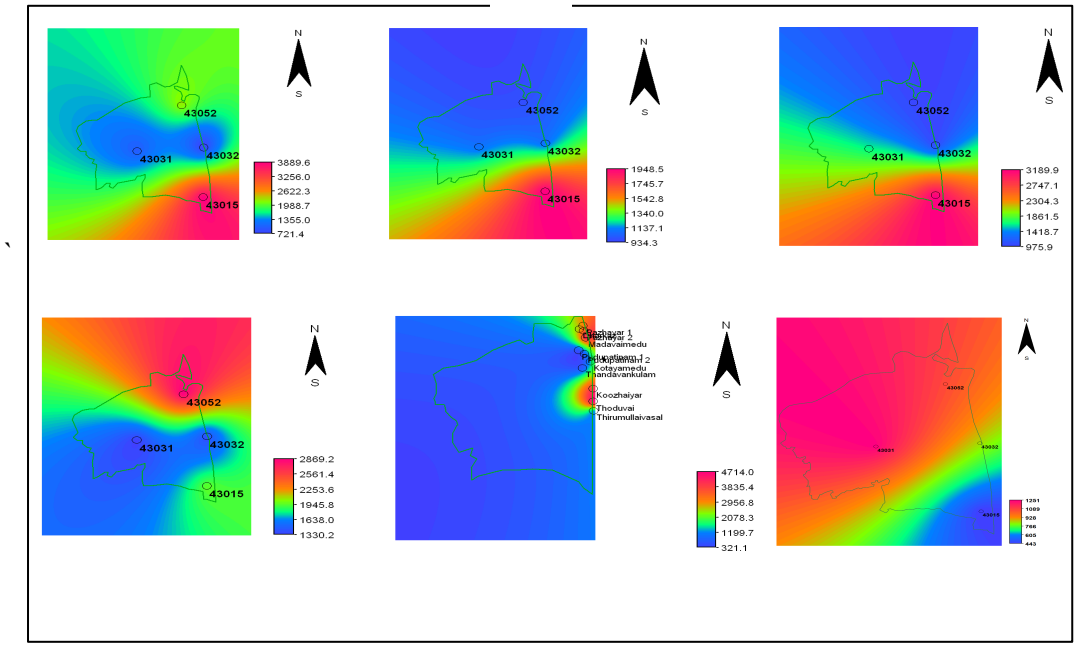

Figure 4 Spatial mapping of Groundwater quality Parameter before and after Tsunami -EC (mhos/cm), 1970-2010

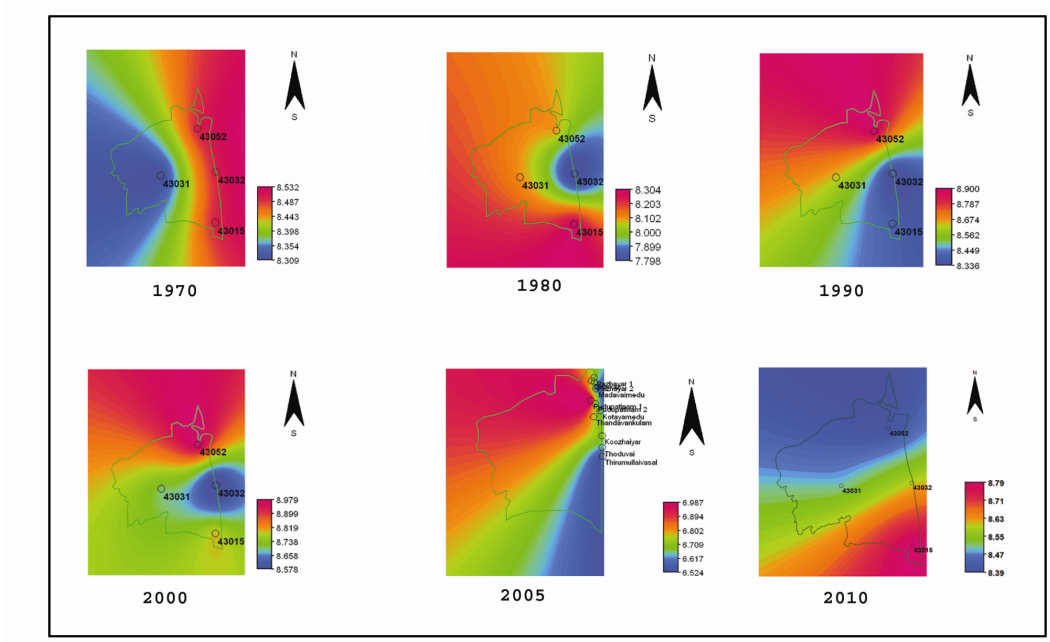

Figure 5 Spatial mapping of Groundwater quality Parameter before and after Tsunami -pH, 1970-2010

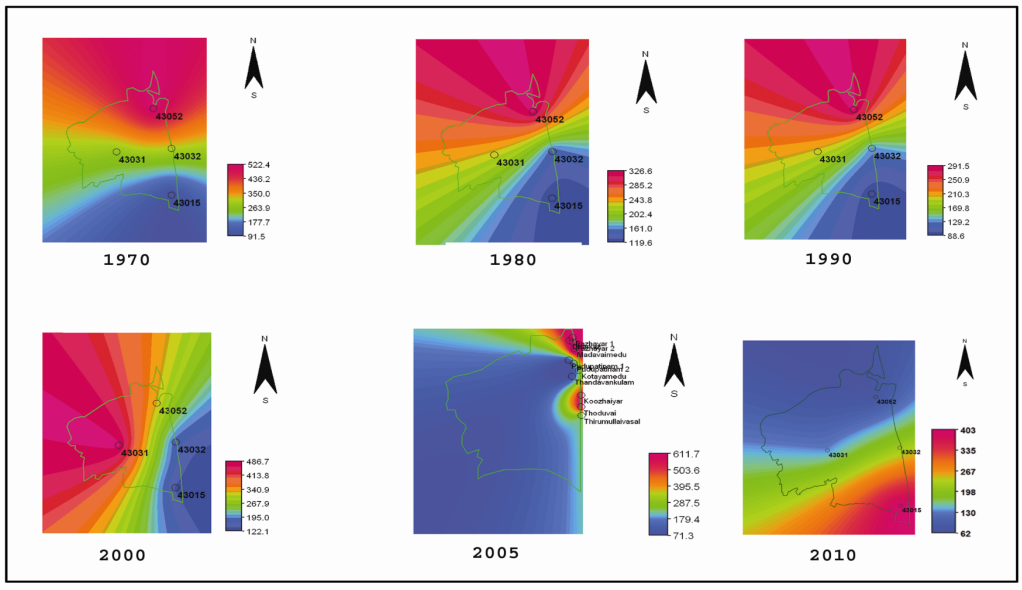

Figure 6. Spatial mapping of Groundwater quality Parameter before and after Tsunami - Na (mg/L), 1970-2010

CONCLUSIONS

The following conclusions were made as,

- The primary data (immediately after Tsunami, 2004) of groundwater samples were collected from the wells shows that the EC ranges from 0.571mhos to 11.16 mhos and the hardness lies between 264 and 2000 mg/L

- Based on the long term (1996 – 2012) comparative study of hydrogeochemical analysis of primary and secondary data of groundwater samples, the following findings are obtained

- The groundwater quality parameters like pH, EC, Chlorides (Cl), Sodium (Na), Hardness, Dissolved Oxygen (DO), percentage salinity and Turbidity present in water samples collected from coastal areas from Sirkali taluk exceeds the limits prescribed by WHO and BIS. The Electrical conductivity (EC) of the groundwater samples immediately after Tsunami from different locations exceeded limits prescribed by WHO

- The maximum EC value obtained from Pazhayar sample is 11.86 mmhos/cm

- Based on the spatial mapping using kriging operation of interpolation of groundwater quality modeling using ILWIS – GIS package, the following values are obtained.
  pH value before and after Tsunami are 8.3 and 6.98 respectively
  EC value before and after Tsunami are 1948 mhos/cm and 4714 mhos/cm
  Na value before and after Tsunami are 527 mg/L and 1631 mg/L
  Cl value before and after Tsunami are 291 mg/L and 611 mg/L
- The quality of water samples collected from different groundwater sources of the study area are affected by Tsunami which is revealed by the test results.

- Contamination of drinking water sources by Tsunami occurred from Saline water incursion which is proved by Georesistivity survey. In general most of the water samples indicated higher concentration of water quality parameters.

- Based on hydro geological conditions, TDS parameters and VES data interpretations, the approximate depth to fresh water-salt water interface and the subsurface lithology were delineated. This study reveals that the average depth to fresh water salt water interface of Sirkali taluk is 4.489 m.

REFERENCES

1. Alagumuthu, G. and Rajan, M. (2010), "Chemo metric studies of water quality parameters of Sankarankoil block of Tirunelveli, Tamilnadu", Journal of Environmental Biology, Vol. 31, 581-586

2. Bhagavathi Perumal, S. and Thamarai, P. (2008), " Analysis of water quality based on Total Dissolved Solids along the coastal area, Kanyakumari, Tamilnadu", Journal of Nature Environment and Pollution Technology, Vol. 8, 123-125

3. CGWB report, (1997), "Ground water resources developments in Nagappattinam district, Tamilnadu

4. Daraigan Sami, G (2011), "Linear correlation analysis study of drinking water quality data for Al-Mukalla City, Hadhramout,Yemen", International Journal of Environmental Sciences, Vol (1),No.7, 1692-1701,ISSN:0976-4402

5. Elango, L., et al, (1992), "Groundwater quality in coastal regions of south Madras", Indian Journal of Environmental Health, Vol. 34, No. 4, 318-325

6. Freeze, A. R. and Cherry, J. A. (1979), "Groundwater", Prentice Hall, Englewood, Cliffs, New Jersey

7. Gadhave, A.G. et al, (2008). "Water Quality Parameters Of Ground Water Near Industrial Areas, Shrirampur (M.S)", Rasayan Journal of Chemistry, 1, 853-855

8. ICMR. (1975), "Maual of standards of quality of drinking water supplies", New Delhi

9. Karanth K.R. (1989), "Hydrogeology", Tata McGraw-Hill, New Delhi.

10. Lawrence, A. R., et al., (1976), "Hydrochemistry and groundwater mixing in part of the Lincolnshire limestone's aquifer, England", Groundwater, Vol. 14, 36-44.

11. Mondal, N. C. et al., (2005), "Assessment of groundwater pollution due to tanneries in and around Dindigul, Tamilnadu, India", Journal of Environmental Geology, Vol. 48 (2), 149-157

12. Pitchammal, V. et al., (2009). "The Study of Water Quality at Madurai, Tamilnadu, India", Nature Environment and Pollution Technology, 8, 355-358

13. Public Works Department (PWD). (2000), "Groundwater Perspectives: A profile of Dindigul District, Tamilnadu", PWD, Govt. of India, Chennai- 600 005, Report 102.

ISSN 8755-6839

SCIENCE OF **TSUNAMI HAZARDS**

Journal of Tsunami Society Internationa

Volume 38 **Number 2** **2019**

IDENTIFICATION OF TSUNAMIGENIC EARTHQUAKE ZONES IN OCEANIC RIDGES AND TRENCHES

O.S. Hammed[1], T.A. Adagunodo[2], M.O. Awoyemi[3], A.B. Arogundade[3], O.D. Ajama[3], F.O. Sapele[1], M.R. Usikalu[2], A.M. Olanrewaju[4], S.A. Akinwumi[2], E.I. Ogunwale[2]

[1] Department of Physics, Federal University, Oye-Ekiti, Nigeria.
[2] Department of Physics, Covenant University, Ota, Nigeria.
[3] Department of Physics, Obafemi Awolowo University, Ile-Ife, Nigeria.
[4] Department of Mathematics, Covenant University, Ota, Nigeria

Email addresses: olaide.hammed@fuoye.edu.ng; theophilus.adagunodo@covenantuniversity.edu.ng; ajobay@oauife.edu.ng

ABSTRACT

Tsunamigenic earthquakes have been known for their near and far field catastrophic impacts on coastal areas near oceanic ridges and trenches, as well as near tectonic faults in closed and semi-enclosed seas. Not all regions of oceanic ridges and trenches are tsunamigenic earthquake zones, but knowledge of the weighted sum of released earthquake energy and of the Gutenberg-Richter relation of the 'a' and 'b' parameters are needed to better identify them as to their potential for tsunami generation. The present analysis was undertaken in order to better identify tsunamigenic zones near oceanic ridges and trenches in the Mid-Atlantic, in the Pacific, in Chile, in Japan, near the Aleutians and along the Peru-Chile trench. The weighted sum of earthquake energy released and of the Gutenberg-Richter relation parameters were evaluated to identify tsunamigenic earthquake zones along these locations. The present analysis of the Gutenberg-Richter relation of the 'a' and 'b' parameters indicates that tsunamigenic earthquakes do not occur frequently along the Aleutian Trench, although the historic record supports that destructive tsunamis have occurred along this region in the past. Of the oceanic ridges, the results of the present analysis indicate that the Mid-Atlantic Ridge is the most active tsunamigenic zone, while of all the oceanic trenches, the Japan Trench is the most active.

Keywords: *b-value, a-value, tsunamigenic, oceanic ridges, oceanic trenches*

1. **INTRODUCTION**

Large earthquakes of relatively shallow focal depth near oceanic ridges and trenches can generate destructive tsunamis. (Adagunodo and Sunmonu, 2015). The term tsunamigenic earthquake was introduced by Kanamori (Kanamori, 1972) for events associated with such destructive waves. Some of the better known historical tsunamigenic earthquakes are the 1994 Java earthquake *(*Bryant, 2008*)*, the 1996 Chimbote earthquake (Polet, 2000), the 2006 Pangandaran earthquake and tsunami *(*Ammon et al., 2006), and the 1570 to 2015 tsunamis/earthquakes in Chile (Adagunodo et al., 2018a). Tsunamigenic earthquakes occur frequently but extremely destructive events for certain areas may occur as long apart as every 800 years (Pararas-Carayannis, 2011; Adagunodo et al. 2018a). These kinds of earthquakes are those that usually exceed 7.5 Richter magnitudes.

Most disastrous tsunamis are generated by shallow, great earthquakes near tectonic subduction zones (Figure 1). More than 80% of the world's tsunamis occur along subduction zones in the perimeter in the Pacific, often referred to as the "Ring of Fire". Tsunamis were particularly catastrophic impacts in certain areas in the world. For example, the tsunami generated by the 27 March1964 Alaska earthquake, damaged heavily communities along the Gulf of Alaska, Kodiak Island and Prince William Sound area as well as in the Bay of Valdez - killing 107 people (Pararas-Carayannis, 1967). On 17 July 1998, four villages on Papua - New Guinea's north coast were almost entirely swept away by tsunami waves. The 1896 Sanriku (Japan) earthquake generated a 35 meter high tsunami that washed away 10,000 homes and killed 26,000 people. The 1964 Alaska earthquake created a 7 meter high tsunami that struck a power station, plunging in darkness the city of Hilo on the island of Hawaii. In addition, Adagunodo et al. (2018a) reported that tsunamis and earthquakes within recorded history have rendered about 1.8 million people homeless.

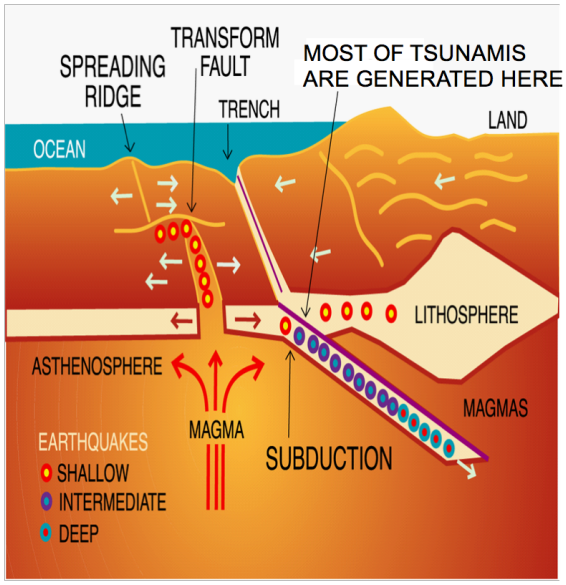

Figure 1: Generation of tsunamigenic earthquakes at subduction zone.

A standard method in providing early warnings for tsunami is based on data that identifies an earthquake as potentially tsunamigenic and is able to predict the possible size and destructiveness of the waves (Tsuboi, 2000). In the present study, the weighted sum of earthquake energy released and the frequency-magnitude distribution of the earthquakes were used to identify the tsunamigenic earthquake zones in three oceanic ridges (Chile Ridge, Mid-Atlantic Ridge and Pacific Ridge) and three trenches (Aleutian Trench, Japan Trench and Peru-Chile Trench) respectively. Identification of earthquake occurrences in such regions facilitates the issuance of tsunami warnings (Adagunodo and Sunmonu, 2015). Analyses of seismically active zones have been reported by some researchers (Hammed et al., 2013; Awoyera et al., 2016; Awoyemi et al., 2017; Awoyera et al., 2017; Adagunodo et al., 2018b; and Hammed et al., 2018).

2. DATA ACQUISITION, DESCRIPTION AND METHOD

The data used for this study were obtained from the earthquake catalogue of the Advance National Seismic System (ANSS) hosted by the Northern California Earthquake Data Centre U.S.A in a readable format. The data comprised of earthquakes occurring along the mid-ocean ridges and trenches with magnitudes of $2.0 \leq M \leq 9.0$ from January 1, 1978 to December 31, 2017 (40-year data period). The data for each earthquake gave the date and time of occurrence, the latitude and longitude of the epicenter, the depth, the magnitude designation, and source codes and event identification. Using "Compicat" software - an earthquake catalog processing software - the data were sorted out, filtered and analyzed in order to remove errors due to data duplication and mixing.

The oceanic ridges that were studied are shown on the seismicity map in Figure 2, specifically: a) The Chile Ridge from latitude 48^0 to 36^0 S and longitude 110^0 to 75^0 W; b) The Mid Atlantic Ridge from latitude 50^0 S to 20^0 N and longitude 45^0 to 10^0 W; and c) The Pacific Ridge from latitude 68^0 to 58^0 S and longitude 120^0 to 18^0 W.

The oceanic trenches that were studied are also shown in Figure 2. Specifically examined were a) the Aleutian Trench from latitude 51^0 to 53^0 N and longitude 160^0 to 176^0 W.; b) The Japan Trench from latitude 40^0 to 53^0 N and longitude 148^0 to 165^0 E; and c) The Peru - Chile Trench from latitude 15^0 S to 30^0 N and longitude 75^0 to 64^0 E. The parameters that were evaluated were the weighted sum of earthquake energy released and the frequency-magnitude distribution of the earthquakes.

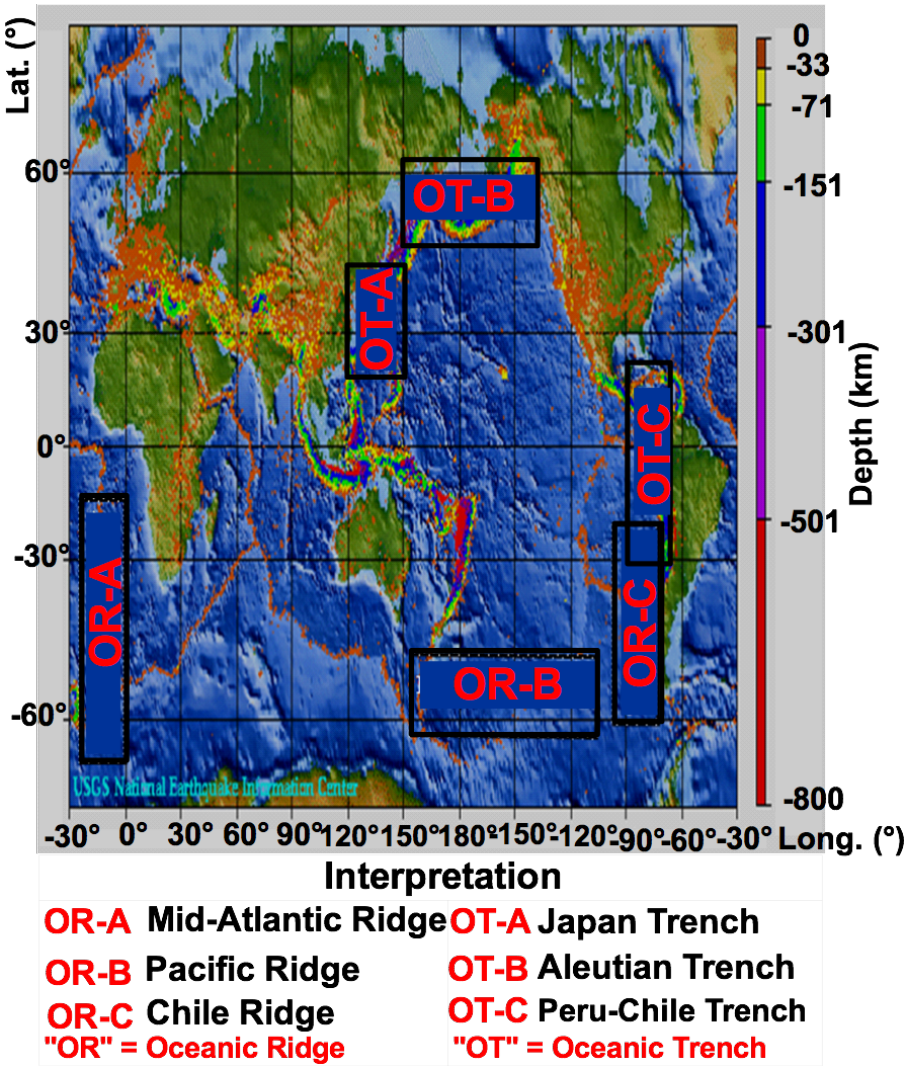

(Source: National Earthquake Information Center (NEIC), US Geological Service)

Figure 2: Map of the global seismicity (1975 – 2010) color-coded by depth

2.1 Method

2.1.1 Evaluation of Weighted Sum of Earthquake Energy Released

In order to study the seismic pattern or hazard of a region, there is a need to investigate the earthquake energy released in the earthquake prone regions to mitigate the future occurrence of earthquakes (Amiri et al., 2008; Ghosh, 2007). The earthquake energy released in oceanic ridges and trenches were plotted against the coordinates of epicenters of the earthquakes in order to understand the seismic activity of the regions (Figures 3 and 4).

2.1.2 Evaluation of Frequency-Magnitude Distribution (FMD) of the Earthquakes

The Frequency-Magnitude Distribution (FMD) - also known as the Gutenberg-Richter relation proposed by Charles Francis Richter and Beno Gutenberg (Richter and Gutenberg, 1944) - is commonly used in the modeling of earthquake hazard, mostly related to the earthquake precursors and probabilistic seismic hazard assessments (Nuannin, 2006; Damanik *et al*. 2010). The FMD describes the number of earthquakes occurring in a given region as a function of their magnitude *M* as:

$$\text{Log N} = \text{a} - \text{bM} \quad (1)$$

where *N* is the cumulative number of earthquakes with magnitudes equal to or greater than *M*, and "*a"* and "*b"* are real constants with values which vary in space and time. The parameter "a" characterizes the general level of seismicity in a given area during the study period i.e. the higher the *a*-value, the higher the seismicity. The parameter "*b"* commonly called the *b*-value has been widely used in the study of seismicity, tectonics, seismic risk estimation and earthquakes prediction. The *b*-value indicates the tectonic character of a region and assumed to depend on the accumulated stress in that region (Nuannin, 2006). Schorlemmer *et al.* (2004) described *b*-value as a stress meter, depending inversely on the differential stress.

For the present work, the FMD of the earthquakes along oceanic ridges and trenches were evaluated by plotting the logarithm of the cumulative number of the earthquakes as a function of their magnitudes. These plots were then fitted with straight lines that best fit the plots (Adagunodo et al. 2018b). The straight lines represent the Gutenberg – Richter equation as shown in Equation 1. The overall "a" and "*b*" values of earthquakes in each study region were obtained as an intercept and a slope of the line of best fit, respectively.

3.0 RESULTS AND DISCUSSION

3.1 Analysis of Weighted sum of Earthquake Energy along Oceanic Ridges

The distribution of weighted sum of earthquake energy released in the Mid Atlantic Ridge as shown in Figure 3a revealed that the earthquake energy released in the ridge is predominantly concentrated in both the southeastern and northeastern part of the ridge. However, the large earthquake energy is prevalent in the northeastern part of the ridge as shown in Figures 3b and 3c. These figures obviously revealed the image of earthquake energy distribution along the epicenter coordinates. The earthquake energy is sparsely concentrated in the southwestern region of the ridge. The extremely large energy in the eastern part of the ridge is an indication that the region is prone to continuous accumulation of oceanic lithospheric plate stress which can generate large earthquakes. A large earthquake within the oceanic ridge can generate a tsunami. The cluster of large earthquake energy in the northeastern part of the ridge is an indication that the region is an earthquake zone that has the potential of generating tsunamis. In the Pacific Ridge, the spatial distribution of earthquake energy released along the ridge is shown in Figure 3d. The latitudinal and longitudinal coordinates of the energy distribution were

also investigated (Figures 3e and f). The weighted sum of earthquake energy is predominantly distributed towards the northern part of the ridge and sparsely distributed towards the southern part of the region as shown in Figures 3d–f. The upper part of the ridge can be regarded as an earthquake prone zone. The spatial distribution of earthquake energy along the ridge reveals a prominent large weighted sum of earthquake energy. Thus, this ridge can also be categorized as being an earthquake zone that can generate tsunamis.

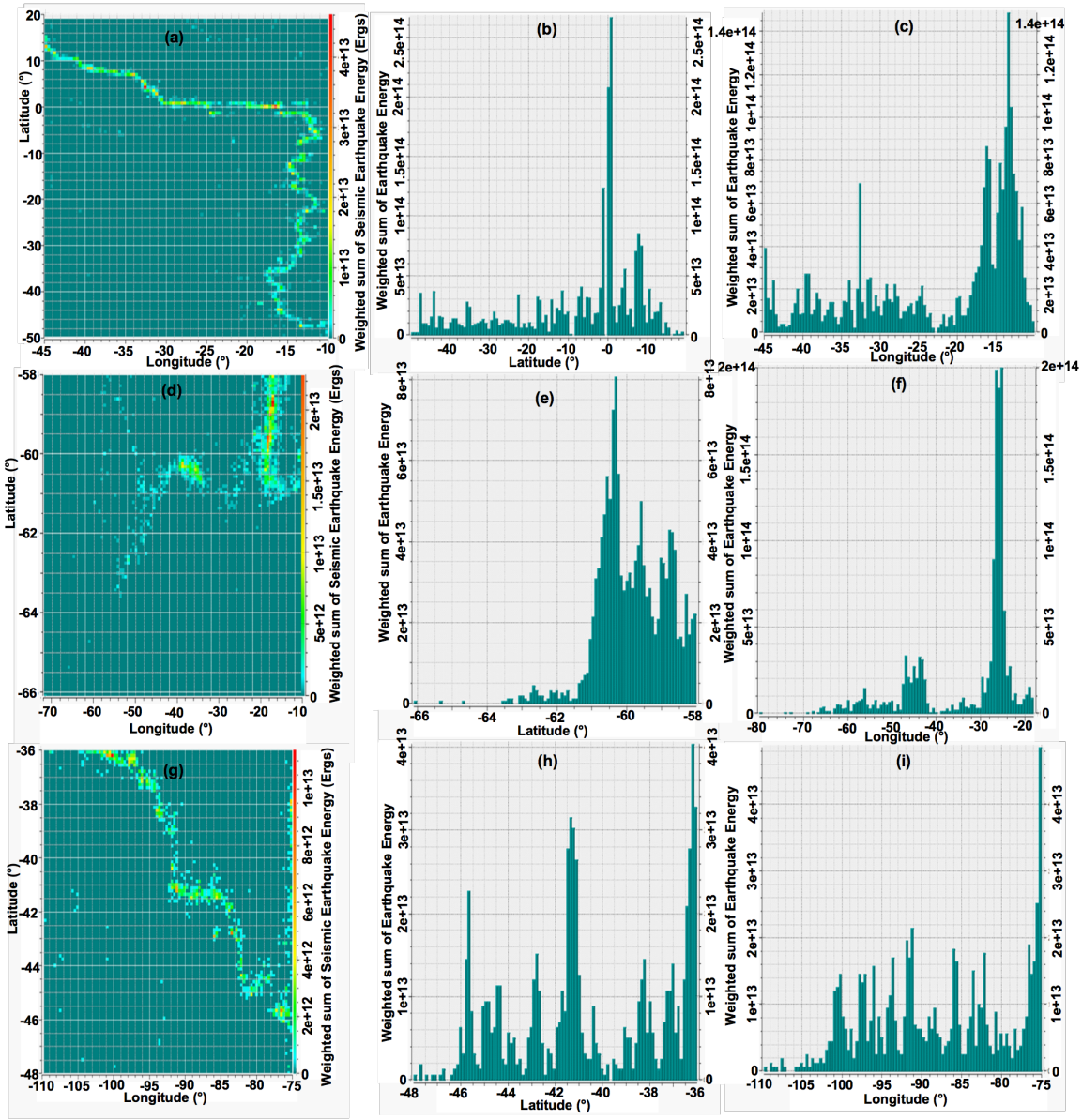

Figure 3: Spatial distribution maps of weighted sum of earthquake energy released. (a) Mid-Atlantic Ridge. (b) Latitudinal coordinate epicenter in Mid Atlantic Ridge. (c) Longitudinal coordinate epicenter in Mid Atlantic Ridge. (d) Pacific Ridge. (e) Latitudinal coordinate epicenter in Pacific Ridge. (f) Longitudinal coordinate epicenter in Pacific Ridge. (g) Chile Ridge. (h) Latitudinal coordinate epicenter in Chile Ridge. (i) Longitudinal coordinate epicenter in Chile Ridge.

The spatial distribution of earthquake energy in the Chile Ridge, as illustrated in Figure 3g, shows that the earthquake energy is evenly distributed across the entire length. The study of both latitudinal and longitudinal coordinates of earthquake epicenters indicates that earthquake energy released on the ridge is evenly distributed (Figures 3h and i). Large earthquake energy seems to be present in the entire region. Therefore, the earthquake energy distribution along the Chile Ridge, indicates that it is a seismically very active earthquake zone that can generate destructive tsunamis.

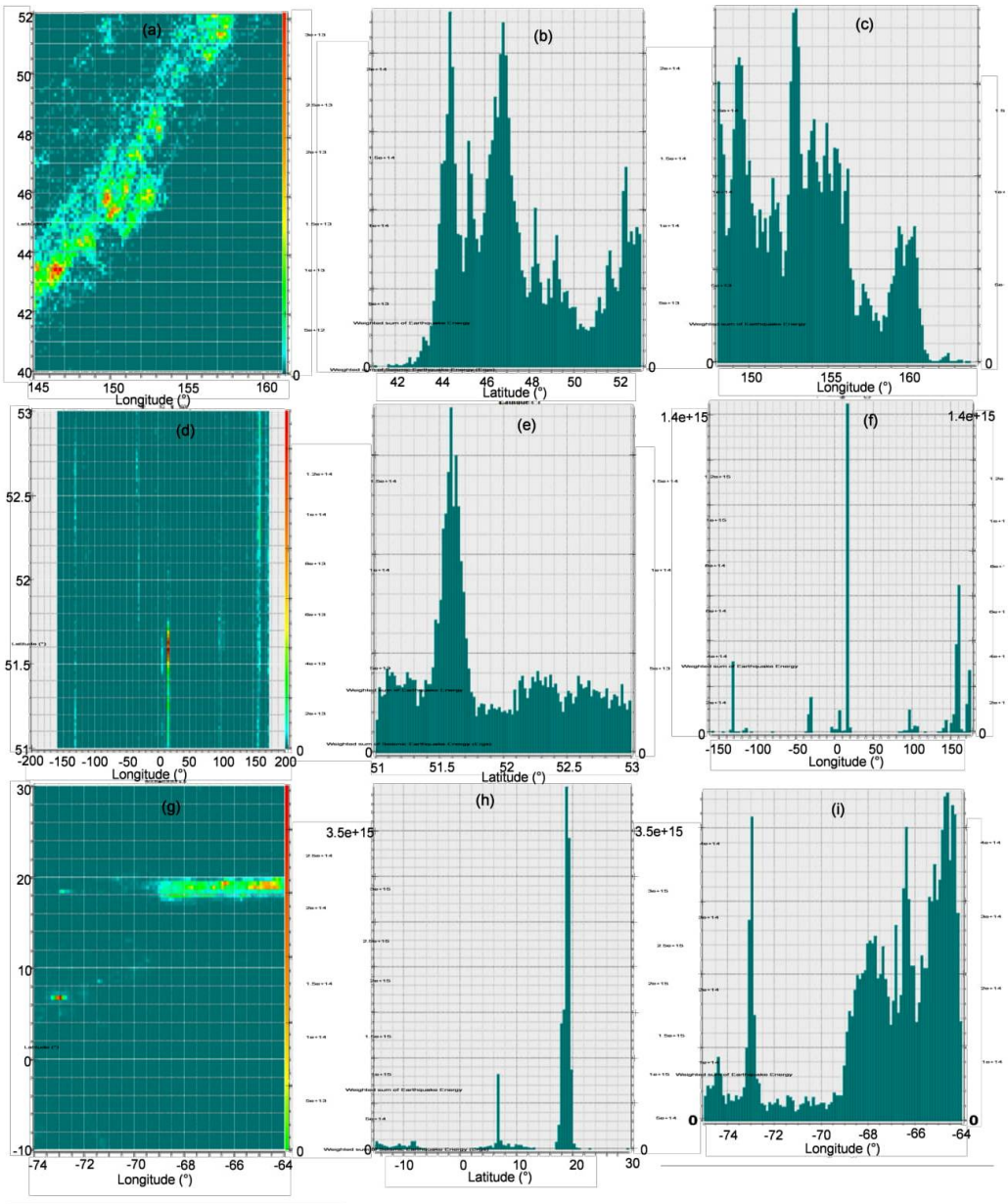

Figure 4: Spatial distribution maps of weighted sum of earthquake energy released. (a) Japan Trench. (b) Latitudinal coordinate epicenter in Japan Trench. (c) Longitudinal coordinate epicenter in Japan Trench. (d) Aleutian Trench. (e) Latitudinal coordinate epicenter in Aleutian Trench. (f) Longitudinal coordinate epicenter in Aleutian Trench. (g) Peru-Chile Trench. (h) Latitudinal coordinate epicenter in Peru-Chile Trench. (i) Longitudinal coordinate epicenter in Peru-Chile Trench.

3.2 Analysis of the Weighted sum of Earthquake Energy along Oceanic Trenches

Figure 4a shows the 2-dimensional image of the weighted sum of earthquake energy along the Japan Trench. The earthquake energy released in this zone is heavily distributed in the northwestern and southwestern regions of the trench, but sparsely distributed in other parts of the trench. Figures 4b and 4c also reveal the image of the energy distribution along the coordinates of the epicenter that corroborates the 2-dimensional image of Figure 4a. Heavy distribution of energy along the Japan Trench indicates large accumulation of stress along this zone. The consequential effect of this can generate tsunamigenic earthquakes within the oceanic floor.

The Aleutian Trench cannot be regarded as tsunamigenic zone based on the fact that the spatial distribution of the weighted sum of earthquake energy in this subduction zone is sparsely concentrated in all the regions of the trench (Figure 4d). Large earthquake energy is seldom released in this trench. In the latitudinal and longitudinal coordinates, only minute portions of the trench experience large earthquake energy as shown in Figures 4e and 4f. The weighted sum of this energy can be regarded as 'negligible' based on its spatial distribution. This implies that this trench can be regarded as a fairly stable region with low seismicity.

Figure 4g, indicates that the earthquake energy distribution along the Peru-Chile Trench only dominates its northeastern part and sparsely the other parts of the trench. Figures 4h and 4i illustrate that the weighted sum of energy released in the trench is very large in the eastern and northern part. This analysis implies that the Peru-Chile Trench can be regarded as tsunamigenic earthquake zone.

3.3 Interpretation of Gutenberg – Richter relation constants in oceanic ridges and Trenches

The frequency magnitude distribution showing "a" and "b" values for the Mid-Atlantic, the Pacific and the Chile Ridges as well as for the Japan, the Peru-Chile, and the Aleutian Trenches (Figures 5a–f) show the Gutenberg – Richter relation parameters (a and b values) in the oceanic ridges and trenches. The "*a"* and "*b"* are real constants with values which vary in space and time. Parameter "a" characterizes the general level of seismicity in a given area during the study period - the higher the *a* value, the higher the seismicity. The parameter "*b"* commonly called the *b*-value has been widely used in the study of seismicity, tectonics, seismic risk estimation and earthquakes prediction. The *b*-value indicates the tectonic character of a region and assumed to depend on the accumulated stress in that region (Nuannin, 2006). Schorlemmer *et al.* (2004) described *b*-value as a stress meter, depending inversely on the differential stress. Therefore, the lower the "b" value, the higher is the tectonic stress in the region (Adagunodo et al. 2018a; b).

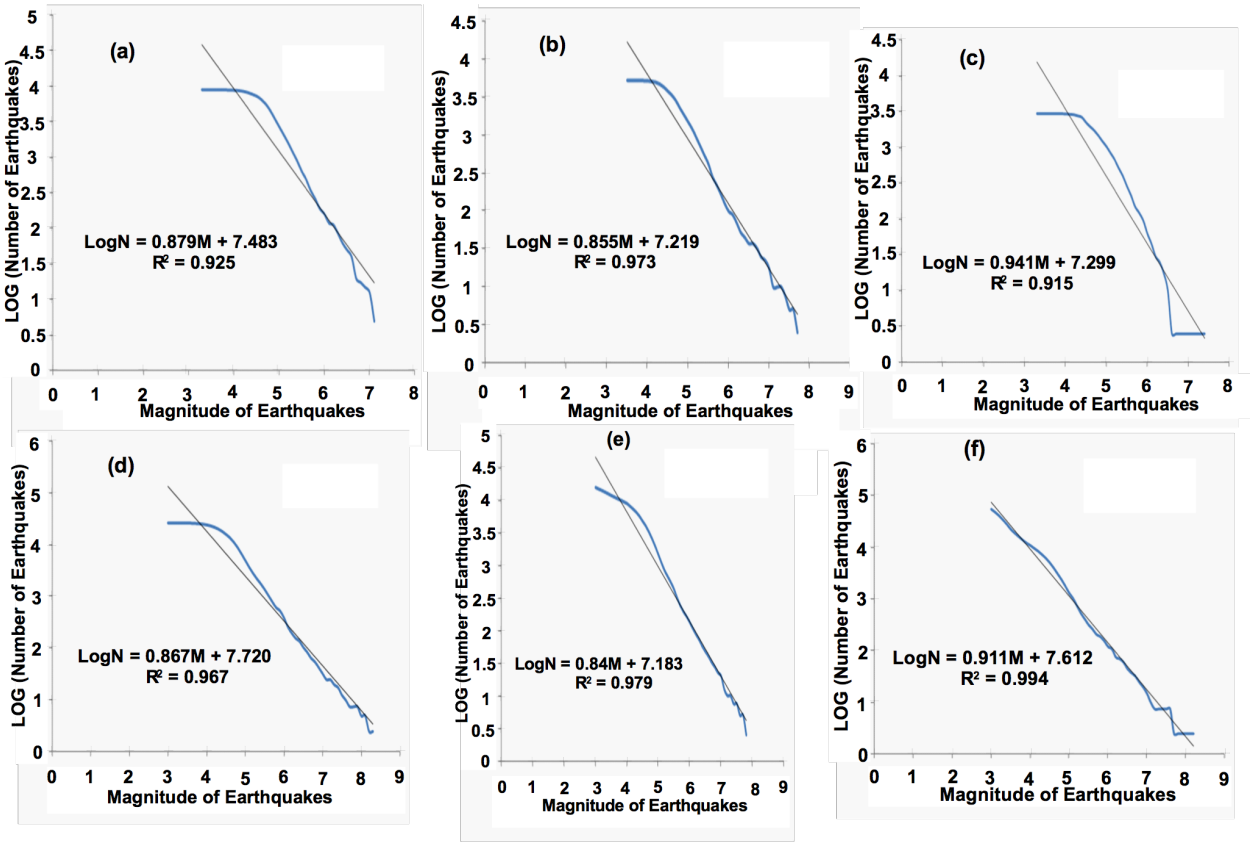

Figure 5: Maps of FMD of earthquakes in the study locations. (a) Mid-Atlantic Ridge (1978-2017). (b) Pacific Ridge (1978-2017). (c) Chile Ridge (1978-2017). (d) Japan Trench (1978-2017). (e) Aleutian Trench (1978-2017). (f) Peru-Chile Trench (1978-2017).

3.4 Interpretation of Gutenberg – Richter "a" value

In the ridges and trenches, the a-value that was obtained is far greater than one. This signifies that there is an increase in the occurrences earthquakes in ridges and trenches. The earthquakes recorded in Mid-Atlantic Ridge outnumbered those recorded in along the Pacific and Chile Ridges respectively. This implies that numerous significant tsunamigenic earthquakes had been occurring in all these ridges but more predominantly in the Mid–Atlantic Ridge. Furthermore, the earthquakes recorded along the Japan Trench outnumbered those recorded along the Aleutian and Peru-Chile Trenches, respectively. This implies that numerous significant tsunamigenic earthquakes had been occurring along all these trenches as well, but more prevalent in the Japan Trench. In comparison, the earthquake events in Trenches outnumbered that of Ridges. Thus, trenches are more prone to earthquakes than the ridges. Computation of a-values from the six study locations is presented in Table 1.

3.5 Interpretation of Gutenberg –Richter "b" value

The low b-values (b << 1) obtained in the ridges and trenches reveal that the rate of tectonic stress accumulation is very high, an indication of increase in the rate of divergence and convergence of lithospheric plates, along the ridges and trenches respectively. The high rate of divergence of tectonic plates in the ridges and convergence in the trenches implies that the lithospheric plates are becoming more unstable and tectonic stress accumulation is increasing in both the ridges and trenches. Therefore, these regions can be regarded as seismogenic zones. Computation of b-values from the investigated ridges and trenches are shown in Table 1.

Table 1: Distribution of a- and b-values in the oceanic ridges and trenches (1978-2017)

Location	a-value	b-value
Mid-Atlantic Ridge	7.483	0.879
Pacific Ridge	7.219	0.855
Chile Ridge	7.299	0.941
Japan Trench	7.720	0.867
Aleutian Trench	7.183	0.840
Peru-Chile Trench	7.612	0.911

3.6 Temporal variation of b-value along the ridges and trenches

Temporal variation of "b" values along the oceanic ridges and trenches as shown in Figures 6a and b revealed that earthquakes of large magnitudes occurred in intervals of low *b*-values. A significant drop in b-value indicates an increase in the stress level. The *b*-value mapping is therefore a useful tool to display variation of stress accumulation over large areas (Awoyemi et al., 2017). In Figures 6a and b, a V-shape curve is experienced as the b-values drop with respect to time, which corresponds to large earthquakes (≥ M6). A rapid decrease in *b*-value with time was observed prior to the occurrence of large earthquakes, and rapid increase in *b*-value was also observed after the occurrence of large earthquakes. Therefore, this anomalous variation of *b*-value with time may be considered as a precursor for earthquake prediction in the ridges and trenches. In Figure 6a, the low temporal *b*-values are associated with earthquakes along the Mid – Atlantic, the Pacific and the Chile Ridges. This is an indication of increase in tectonic stress level in the oceanic ridges. The lowest "b" value was observed for the Mid – Atlantic Ridge. The *b*-value associated with the earthquakes the Pacific Ridge is lower than that of the Chile Ridge. Based on this, the Mid – Atlantic Ridge can be regarded as the most tsunamigenic earthquake zone of all three ridges. In the same vein, Figure 6b revealed low temporal *b*-values in the investigated trenches. The estimations of b-value from the three investigated trenches are in the order: Japan Trench < Peru-Chile Trench < Aleutian Trench. Therefore, Japan Trench can be regarded as the most tsunamigenic earthquake zone of all these trenches.

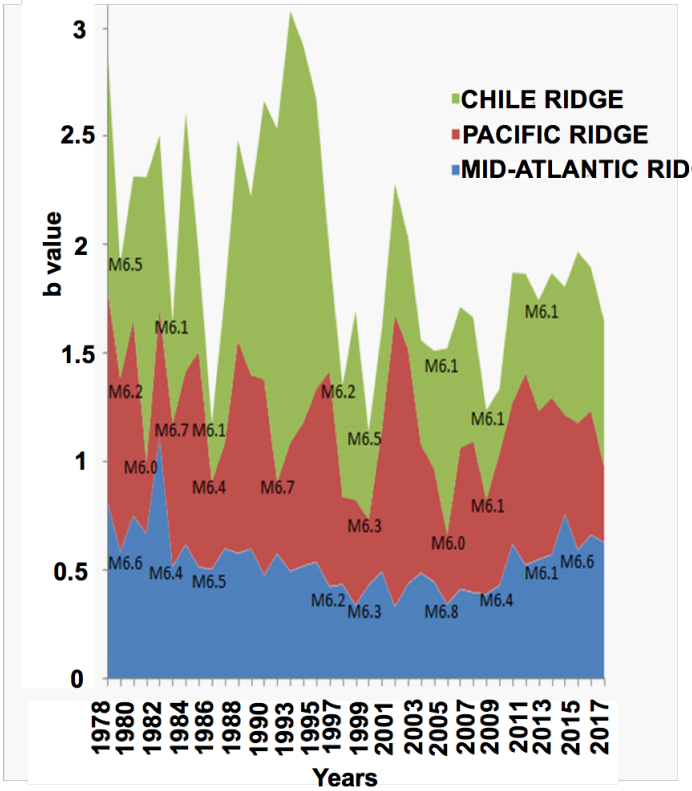

Figure 6a: Temporal variation of b-value in Oceanic Ridges

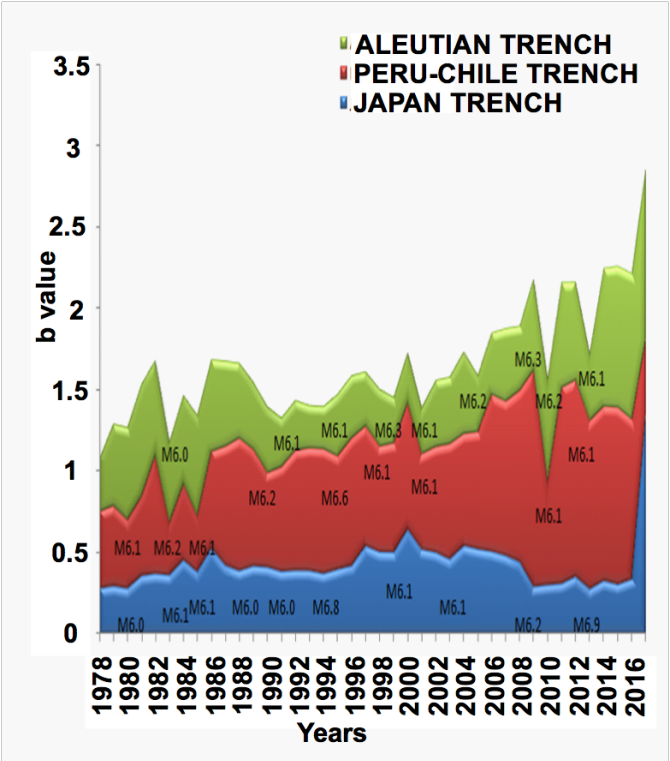

Figure 6b: Temporal variation of b-value in Oceanic Trenches

4.0 CONCLUSIONS

The cluster of large earthquake energy in the northeastern part of the Mid-Atlantic ridge and the northern part of the Pacific Ridge is an indication that the region has high potential for the generation of tsunamis. The spatial distribution of earthquake energy in the Chile Ridge indicates that the earthquake energy released is evenly distributed across the ridge. However, the Chile Ridge can also be regarded as being a region of high tsunamicity. The earthquake energy released in the Japan Trench is heavily distributed in its northwestern and southwestern of the trench and sparsely distributed along the other parts of the trench. The earthquake energy distribution along the Peru-Chile Trench appears to be only concentrated along the northeastern part of the trench and sparsely distributed along its other parts of the trench. This implies that earthquakes along the Japan and Peru-Chile trenches can be regarded as having a high potential to generate tsunamis with greater frequency, while tsunamigenic earthquakes along the Aleutian Trench are less frequent - cannot be regarded as such based on the fact that the spatial distribution of the weighted sum of earthquake energy in this subduction zone is sparsely distributed in all the regions of the trench. Only the Aleutian Trench can be regarded as fairly stable trench (with low seismicity) of all the trenches, because large earthquake energy is only experienced in minute portions of the trench.

The b-values associated with the earthquake in the oceanic Ridges and Trenches were also investigated in order to identify the tsunamigenic zones in the study locations. Low temporal b-values are associated with earthquakes in Mid-Atlantic Ridge, Pacific Ridge and Chile Ridge, an indication of increase in tectonic stress level in the oceanic ridges. Of all the oceanic ridges, The Mid-Atlantic Ridge depicted the least b-value, while the Chile Ridge depicted the highest b-value. Based on this, the Mid-Atlantic Ridge can be regarded as the most tsunamigenic earthquake zone of all the ridges. From the oceanic trenches the Japan Trench depicted the least b-value, while the Aleutian Trench depicted the highest b-value. Therefore, the Japan Trench can be regarded as the most tsunamigenic earthquake zone of all the trenches.

ACKNOWLEDGMENT

We acknowledge the publication support received from Covenant University, Nigeria.

REFERENCES

Abe, K. (1981). *Physical size of tsunamigenic earthquakes of the northwestern Pacific. Phys. Earth Planet. Inter. **27** (3): 194–205.*

Adagunodo T.A. and Sunmonu L.A. (2015). Earthquake: a Terrifying of all Natural Phenomena. Journal of Advances in Biological and Basic Research. 01(1): 4–11.

Adagunodo T.A., Oyeyemi K.D., Hammed O.S., Bansal A.R., Omidiora J.O., Pararas-Carayannis G. (2018a). Seismicity Anomalies of M 5.0 + Earthquakes in Chile during 1965 – 2015. Science of Tsunami Hazards, 37(2): 130 – 156. http://www.tsunamisociety.org/STHVol37N2Y2018.pdf.

Adagunodo T.A., Lüning S., Adeleke A.M., Omidiora J.O., Aizebeokhai A.P., Oyeyemi K.D., Hammed O.S. (2018b). Evaluation of 0 ≤ M ≤ 8 Earthquake Data Sets in African-Asian Region during 1966 – 2015. Data in Brief, 17C: 588 – 603. https://doi.org/10.1016/j.dib.2018.01.049.

Amiri G.G., Razeghi H.R., RazavianAmreiS.A., Aalaee H., Rasouli S.M. (2008). SeismicHazard Assessment of Shiraz, Iran.Journal of Applied Sciences. 8:38-48.

Ammon, C.J.; Kanamori H.; Lay T.; Velasco A.A. (2006). The 17 July 2006 Java tsunami earthquake *(PDF). 33. American Geophysical Union: L24308.* Bibcode:2006GeoRL..3324308A. doi:10.1029/2006GL028005. Retrieved 23 July 2011.

Awoyemi M.O., Hammed O.S., Shode O.H., Olurin O.T., Igboama W.N., Fatoba J.O. (2017). Investigation of b-value variations in the African and parts of Eurasian plates. Journal of Tsunami Society International, 36(2): 86 – 99.

Awoyera P. O., Ogundeji J. and Aderonmu P.A. (2016). *Simulated Combined Earthquake and Dead Load Lateral Resistance Building Systems using Nigeria Seismic Data. Journal of Materials and Environmental Science, 7 (3): 781-789. ISSN 885-894.*

Awoyera P.O., Ngene B.U., Adeyemi G.A., Aderonmu P.A. (2017). *Mitigating Ground Shaking Construction Activities in Coastal Cities of Nigeria: An Earthquake Preventive Measure. In: Earthquakes: Monitoring Technology, Disaster Management and Impact Assessment. Nova Science Publishers, Inc.. ISBN 978-1536103427.*

Bryant, E. (2008). *5-Earthquake-generated tsunami.* Tsunami: the underrated hazard *(2 ed.). Springer. pp. 129–138.* ISBN 978-3-540-74273-9. Retrieved 19 July 2011.

Damanik, R., Andriansyah, Putra, H. K., Zen, M. T. (2010). Variations of b-values in the Indian Ocean-Australian Plate Subduction in South Java Sea. Proceedings of the Bali 2010International Geosciences Conference and Exposition, Bali, Indonesia: 19 – 22

Ghosh A. (2007) Earthquake frequency-magnitude distribution andinterface locking at the middle America subduction zone nearNicoya Peninsula Costa Rica Georgia institute of technology.http://smartech.gatech.edu/handle/1853/16288

Hammed O.S., Popoola O.I., Adetoyinbo A.A., Awoyemi M.O., Adagunodo T.A., Olubosede O., Bello A.K. (2018). Peak Particle Velocity Data Acquisition for Monitoring Blast Induced Earthquakes in Quarry Sites. Data in Brief, 19: 398 – 408. https://doi.org/10.1016/j.dib.2018.04.103.

Hammed O.S., Popoola O.I., Adetoyinbo A.A., Awoyemi M.O., Badmus G.O., Ohwo O.B. (2013). Focal depth, magnitude, and frequency distribution of earthquakes along Oceanic Trenches. Earthquake Science, 26: 75 – 82.

Ishibashi, K. (2004). Status of historical seismology in Japan. *Annals of Geophysics. 47 (2/3): 339–368*. Retrieved 22 November 2009.

Kanamori, H. (1972). Mechanism of tsunami earthquakes. *Physics of the Earth and Planetary Interiors. 6: 346–359.* Bibcode*:*1972PEPI....6..346K. doi*:* 10.1016/0031-9201(72)90058-1. Retrieved 19 July 2011.

Kanamori, Hiroo*;* Kikuchi, Masayuki *(1993).* The 1992 Nicaragua earthquake: a slow tsunami earthquake associated with subducted sediments. Nature. *361 (361): 714–716.* Bibcode*:*1993Natur.361..714K. doi*:*10.1038/361714a0.

Pararas-Carayannis, G. (1967). Source Mechanism Study of the Alaska Earthquake and Tsunami of 27 March 1964, The Water Waves. Pacific Science. Vol. XXI, No. 3, July 1967.

Pararas-Carayannis, G. (2007). The Earthquake and Tsunami of 2 September 1992 in Nicaragua. Archived *from the original on 17 May 2008*. Retrieved 2008-06-09.

Pararas-Carayannis, G. (2011). The earthquake and tsunami of July 21, 365 AD in the EasternMediterranean Sea - Review of impact on the ancient world - assessment of recurrenceand future impact. 30 (4): 286.

Polet, J. & Kanamori H. (2000). Shallow subduction zone earthquakes and their tsunamigenic potential***. Geophysical Journal International. Royal Astronomical Society. 142: 684–702.*** Bibcode*:*2000GeoJI.142..684P. doi*:*10.1046/j.1365-246X.2000.00205.x. **Retrieved 23 July 2011.**

Schorlemmer, D., S. Wiemer, and M. Wyss 2004. Earthquake Statistics at Parkfield I: Stationarity of b-values. Journal of Geophysical Research 109

Tanioka, Y.; Seno T. (2001). Sediment effect on tsunami generation of the 1896 Sanriku tsunami earthquake. *Geophysical Research Letters. 28 (17): 3389 - 3392.*

Tsuboi, S. (2000). Application of M_{wp} to tsunami earthquake. *Geophysical Research Letters. American Geophysical Union. 27 (19).* Bibcode:2000GeoRL..27.3105T. doi:10.1029/2000GL011735. Retrieved 19 July 2011.

ISSN 8755-6839

SCIENCE OF TSUNAMI HAZARDS

Journal of Tsunami Society International

Volume 38 Number 1 2019

TSUNAMI SOCIETY INTERNATIONAL, 1741 Ala Moana Blvd. #70, Honolulu, HI 96815, USA.

WWW.TSUNAMISOCIETY.ORG

ISSN 8755-6839

SCIENCE OF TSUNAMI HAZARDS

Journal of Tsunami Society International

Volume 38 Number 1 2019

TSUNAMI SOCIETY INTERNATIONAL, 1741 Ala Moana Blvd. #70, Honolulu, HI 96815, USA.

WWW.TSUNAMISOCIETY.ORG